
Machine Learning for highly oscillatory differential equations

Maxime Bouchereau¹

¹IRMAR, Université de Rennes

January 21, 2026

Keywords: Highly oscillatory differential equation, Slow-fast decomposition, Micro-Macro method, auto-encoder, numerical method, averaging theory.

Abstract

Highly oscillatory differential equations, commonly encountered in multi-scale problems, are often too complex to solve analytically. However, several numerical methods have been developed to approximate their solutions. Although these methods have shown their efficiency, the first part of the strategy often involves heavy pre-computations from averaging theory. In this paper, we leverage neural networks (machine learning) to approximate the vector fields required by the pre-computations in the first part, and combine this with micro-macro techniques to efficiently solve the oscillatory problem. We illustrate our work by numerical simulations.

1 Introduction

Highly oscillatory differential equations are frequently used to model phenomena exhibiting a multiscale behavior with periodic dependence [14, 10]. However, most of these equations cannot be solved analytically. While various numerical methods exist for autonomous differential equations [4, 7, 9, 22, 26, 32], they are not well-suited for highly oscillatory equations due to their stiffness.

Although the methods mentioned above are not suitable for solving highly oscillatory ODEs, the analytical properties of these differential equations [10, 11, 31] can be leveraged to develop effective numerical techniques. In particular, uniformly accurate methods are particularly powerful, as their error bounds do not depend on the stiffness parameter [14, 15].

These methods rely on transforming the studied dynamical system into a modified form to enable the correct application of numerical techniques. For instance, preliminary computations

often involve the slow-fast decomposition, which separates the multiscale dynamics of the system into slow and fast components. However, such a decomposition provides only an approximation of the original problem and may not be solely used to construct uniformly accurate (UA) numerical schemes. Two approaches have been developed to remedy this deficiency. The first is based on micro-macro decomposition techniques which allow for UA schemes although it increases by a factor 2 the dimension of the problem. The second is based on pullback technique enjoys some geometric properties of the system although it induces some additional computations (inversion of a linear operator) [14].

Although these methods are highly accurate, they require preliminary computations to transform the original dynamical system. For many systems, these transformations involve formal calculations, which can result in significant computational costs [10, 11].

The main idea of this work is to combine the theory of highly oscillatory differential equations with machine learning techniques and in particular neural networks. Given a highly oscillatory differential equation, the slow-fast decomposition of the equation is first learned by extensive simulations and then approximated by inference from a neural network. Since the slow dynamics is described by an autonomous differential equation, the theory of modified equations [23] is used to learn the slow dynamics. Once this representation of the slow-fast decomposition has been obtained, it is used to solve the whole equation via the micro-macro decomposition for any initial value prescribed in a *learnt* range of phase space.

1.1 Scope of the paper

The paper is structured into two main sections: Section 2 introduces the technique and presents the associated convergence results, while Section 3 highlights numerical experiments that demonstrate the properties of the proposed schemes.

Subsection 2.1 describes the strategy for integrating machine learning with averaging theory to solve highly oscillatory differential equations. The central concept is to emulate the *slow-fast* decomposition using neural networks. This method requires the generation of exact data via a highly accurate yet computationally intensive numerical integrator. The data is then used to train neural networks to learn the decomposition by minimizing a $Loss_{Train}$ error function. This approach employs modified equation theory for modeling slow dynamics and an auto-encoder structure for fast dynamics. Moreover, we propose a method based on the micro-macro decomposition that avoids the need for additional training, leading to uniformly accurate approximations. Lastly, an alternative method designed for highly oscillatory autonomous systems is introduced, which eliminates the dependency on an auto-encoder.

Subsection 2.2 focuses on error analysis, providing bounds between exact and approximated solution. First method gives error bound dominated by learning errors of elements of the *slow-fast* decomposition and exponential error w.r.t. ε , providing a good approximation of the solution for small values of ε . Second method based on micro-macro decomposition gives error bounds dominated by learning errors and step size, providing uniformly accurate bounds. Then, alternative method (reserved for oscillatory autonomous systems) provides similar error bounds to first method).

In section 3, numerical experiments are made. For first and second method, we learn the modified averaged field by using Forward Euler and midpoint schemes, and illustrate that elements of *slow-fast* and micro-macro decomposition can properly be approximated for different dynamical systems. For autonomous systems, the experiments include a comparison with the classical method

based on the *slow-fast* decomposition.

1.2 Related work

Connections between differential equations, machine learning, and multiscale problems have been investigated in numerous studies. The relationship between differential equations and machine learning primarily involves learning hidden dynamics from collected data using regression techniques [6, 19] or statistical methods [29, 33]. In contrast, the connection with multiscale problems largely focuses on learning solutions [25].

Modified equation coupling. The connection to modified equation theory has been utilized to study the learning of hidden dynamics in differential equations [19, 36]. Offen et al. extended this approach to learn Hamiltonian functions [30].

Neural network structure and geometric properties. To preserve specific properties of equations, various neural network architectures have been developed. For maintaining asymptotic properties in multiscale equations, Jin et al. employed Physics-Informed Neural Networks (PINNs) [25]. Other architectures have also been proposed for multiscale equations [27, 28, 34], such as Convolutional Neural Networks (CNNs) [35]. To ensure the preservation of geometric properties like Hamiltonian vector fields [16], Hamiltonian Neural Networks have been used [17, 20]. Additionally, reciprocal mappings can be learned effectively using auto-encoders. For example, Jin et al. applied auto-encoders to learn Poisson systems [24]. Moreover, Zhu et al. have developed a method to learn Volume-Preserving vector fields [37].

Approximation by Neural Networks. Accurately approximating functions using neural networks has led to error estimates. Anastassiou [1, 2] established convergence rates for approximating functions that map to finite- and infinite-dimensional vector spaces. These rates depend on the number of parameters and the input dimensionality. By treating neural networks as functional spaces, error bounds have been derived [18, 21]. In a related study, Bach [3] provided error estimates by considering neural networks as elements within a Hilbert space. An important challenge highlighted by Mallat [8] is the curse of dimensionality: as the dimensionality of the vector field increases, the rate of convergence slows, requiring more parameters and data to achieve satisfactory learning outcomes in high-dimensional spaces compared to low-dimensional ones.

2 Approximate solutions of highly oscillatory differential equations with machine learning

Consider an highly oscillatory differential equation of the form

$$\begin{cases} \dot{y}^\varepsilon(t) &= f\left(\frac{t}{\varepsilon}, y^\varepsilon(t)\right) \in \mathbb{R}^d, & t \in [0, T] \\ y^\varepsilon(0) &= y_0 \end{cases} \quad (1)$$

where $f : \mathbb{R} \times \mathbb{R}^d \rightarrow \mathbb{R}^d$ is assumed to be sufficiently smooth and 2π -periodic with respect to its first variable. Additionally, the parameter $\varepsilon \in (0, 1]$ introduces high oscillations. By the Cauchy-Lipschitz theorem, the existence and uniqueness of a solution are guaranteed for any initial $y_0 \in \mathbb{R}^d$. Our goal is to approximate the solution over the interval $[0, T]$ at discrete times points $t_n = nh$, where $0 \leq n \leq N$, with $h = \frac{T}{N}$ representing the step size and N the number of discretization points, with a uniform accuracy with respect to $\varepsilon \in]0, 1]$.

2.1 General strategy

As outlined in the Introduction, we will use neural networks to approximate the *slow-fast* decomposition for solving (1), particularly in cases where the parameter ε is small. Then, we use methods based on a micro-macro decomposition to provide approximations that are valid for all $\varepsilon \in]0, 1]$ and that enjoy uniform accuracy (UA) with respect to ε .

2.1.1 Slow-fast decomposition

Consider $t \mapsto \varphi_t^f(y_0)$, the exact flow corresponding to the equation (1). It is known [12] that one may construct an approximation of $t \mapsto \varphi_t^f(y_0)$ using the following decomposition:

$$\varphi_t^f(y_0) \approx \phi_{\frac{t}{\varepsilon}}^\varepsilon(\psi_t^\varepsilon(y_0)) \quad (2)$$

where $\tau \mapsto \phi_\tau^\varepsilon$ is 2π -periodic, $\phi_0^\varepsilon = \text{Id}^1$ and $\phi^\varepsilon = \text{Id} + O(\varepsilon)$. $\phi^\varepsilon : (\tau, y) \mapsto \phi_\tau^\varepsilon(y)$ introduces high oscillations while $t \mapsto \psi_t^\varepsilon$ results in global drift. $t \mapsto \psi_t^\varepsilon(y_0)$ is the solution of an autonomous differential equation with an associated vector field, denoted F^ε , called the *averaged field*. ϕ^ε and F^ε are usually expressed as formal series expansions in terms of ε :

$$\phi_\tau^\varepsilon(y) = y + \sum_{j=1}^{+\infty} \varepsilon^j \tilde{\phi}_j(\tau, y) \quad \text{and} \quad F^\varepsilon(y) = \langle f \rangle(y) + \sum_{j=1}^{+\infty} \varepsilon^j F_j(y), \quad (3)$$

where $\langle f \rangle$ is the *average field* defined as

$$\langle f \rangle(y) := \frac{1}{2\pi} \int_0^{2\pi} f(\tau, y) d\tau, \quad (4)$$

and the coefficient functions $\tilde{\phi}_j$ and F_j depend on derivatives of f and $\langle f \rangle$. However, the formula referenced as equation (2) may not hold because ϕ^ε and F^ε are defined through formal series that typically do not converge. Despite the non-convergence of the formal series (3), it is possible to construct an approximation of the slow-fast decomposition. Specifically, for all $n \in \mathbb{N}$, let $F^{\varepsilon, [n]}$ and $\phi^{\varepsilon, [n]}$ represent the truncation of F^ε and ϕ^ε obtained by neglecting terms of order $O(\varepsilon^{n+1})$ terms. According to averaging theory (see Chartier et al. [11, 12]), there exists $\varepsilon_0 > 0$ such that, for all $\varepsilon \in]0, \varepsilon_0]$, there is an $n_\varepsilon \in \mathbb{N}$ such that, for all $t \in [0, T]$,

$$\left| \varphi_t^f(y_0) - \phi_{\frac{t}{\varepsilon}}^{\varepsilon, [n_\varepsilon]} \left(\varphi_t^{F^{\varepsilon, [n_\varepsilon]}}(y_0) \right) \right| \leq M e^{-\frac{\beta \varepsilon_0}{\varepsilon}} \quad (5)$$

for some constants $M, \beta > 0$ independent of ε . Since the error bound decays very rapidly as $\varepsilon \rightarrow 0$, this decomposition provides an accurate approximation of the solution for small values of ε . However, this approximation does not hold for values of ε close to 1. Consequently, we need uniformly accurate methods for all values of $\varepsilon \in]0, 1]$.

¹The assumption $\phi_0^\varepsilon = \text{Id}$ arises from stroboscopic averaging [14]. An alternative convention, standard averaging, considers the average $\langle \phi^\varepsilon \rangle = \text{Id}$.

2.1.2 Micro-Macro decomposition

Although the *slow-fast* decomposition is efficient for small values of the parameter ε , it does not provide a uniformly accurate approximation of the solution with respect to ε due to the exponential error described in the referenced estimate (5). To address this issue, the micro-macro decomposition, as outlined by Chartier et al. [14] leverages the multiscale structure of the equation. This approach decomposes the solution into a *slow-fast* component and a remainder. By considering $\phi^{[p]}$ and $F^{[p]}$ as truncations of ϕ^ε and F^ε , respectively, where terms of order $\mathcal{O}(\varepsilon^{p+1})$ are neglected, the following result holds for all $t \in [0, T]$:

$$y^\varepsilon(t) = \phi_{\frac{t}{\varepsilon}}^{[p]}(v(t)) + w(t), \quad (6)$$

where (v, w) is the solution of the micro-macro system, where the second equation is obtained by using (1) and chain rule:

$$\begin{cases} \dot{v}(t) &= F^{[p]}(v(t)) \\ \dot{w}(t) &= f\left(\frac{t}{\varepsilon}, \phi^{[p]}(v(t)) + w(t)\right) - \frac{1}{\varepsilon} \left(\frac{\partial}{\partial \tau} \phi_{\frac{t}{\varepsilon}}^{[p]}\right)(v(t)) - \left(\frac{\partial}{\partial y} \phi_{\frac{t}{\varepsilon}}^{[p]}\right)(v(t)) F^{[p]}(v(t)), \end{cases} \quad (7)$$

with $(v, w)(0) = (y^\varepsilon(0), 0)$. Using a numerical integrator of order p for this system produces an approximate solution of order p , denoted by $(v_n, w_n)_{n \in \mathbb{N}}$, with respect to the step size h :

$$\max_{0 \leq n \leq N} \left| \phi^{[p]}(v(t_n)) + w(t_n) - \phi^{[p]}(v_n) - w_n \right| \leq \overline{M} h^p, \quad (8)$$

where the constant \overline{M} is independent of ε and of h . This ensures a uniformly accurate approximation, making the micro-macro method a *Uniformly Accurate* (UA) method.

2.1.3 Machine learning method

The primary goal of this paper is to approximate the mapping $(\tau, y, \varepsilon) \mapsto \phi_\tau^{\varepsilon, [n_\varepsilon]}(y)$ and the flow $(t, y, \varepsilon) \mapsto \varphi_t^{F^{\varepsilon, [n_\varepsilon]}}(y)$ using neural networks, with the aim of achieving a structure for the approximated solution analogous to (2).

Since the flow $(t, y, \varepsilon) \mapsto \varphi_t^{F^{\varepsilon, [n_\varepsilon]}}(y)$ is associated with following autonomous differential equation

$$\begin{cases} \dot{z}(t) &= F^{\varepsilon, [n_\varepsilon]}(z(t)) \\ z(0) &= y_0, \end{cases} \quad (9)$$

backward error analysis (also known as modified equation theory [23]) can be applied to approximate solutions of equation (9). Using a numerical method Φ_h of order p with a given step size h , let $\widetilde{F}_h^{\varepsilon, [n_\varepsilon]}$ denote the modified field $F^{\varepsilon, [n_\varepsilon]}$ corresponding to Φ_h and $\widetilde{F}_h^{\varepsilon, [n_\varepsilon], [q]}$ represent the truncation of $\widetilde{F}_h^{\varepsilon, [n_\varepsilon]}$ at order h^{p+q-1} [5, 23]. Then, for any compact set $\mathbb{K} \subset \mathbb{R}^d$ and $y \in \mathbb{K}$, we have:

$$\left| \varphi_h^{F^{\varepsilon, [n_\varepsilon]}}(y) - \Phi_h^{\widetilde{F}_h^{\varepsilon, [n_\varepsilon], [q]}}(y) \right| \leq \overline{C} h^{p+q-1}. \quad (10)$$

Next, we approximate $\widetilde{F_h^{\varepsilon, [n_\varepsilon], [q]}}$ using a neural network, denoted by F_θ , which can be interpreted as a perturbation of the averaged field:

$$F_\theta(y, h, \varepsilon) = \langle f \rangle + R_{\theta, F}(y, h, \varepsilon) \quad (11)$$

where the perturbation $R_{\theta, F}$ is modeled as a multilayer perceptron (MLP). Structure of F_θ follows both averaged field (3) and modified field structures [5, 23].

Furthermore, we must account for the high-oscillation generator described by the map $(\tau, y, \varepsilon) \mapsto \phi_\tau^\varepsilon(y)$. To get the autonomous equation from the solution of the initial equation, it is necessary to approximate both $\phi_\tau^{\varepsilon, [n_\varepsilon]}$ and its inverse². For this purpose, an auto-encoder consisting of a pair of neural networks, $(\phi_{\theta,+}(\tau, y, \varepsilon), \phi_{\theta,-}(\tau, y, \varepsilon))$ is used to approximate $(\phi_\tau^\varepsilon(y), (\phi_\tau^\varepsilon)^{-1}(y))$. To preserve the structure of ϕ^ε and its inverse, as required by stroboscopic averaging, both neural networks are designed as perturbations of the identity:

$$\phi_{\theta,+}(\tau, y, \varepsilon) = y + \varepsilon [R_{\theta,+}(\cos(\tau), \sin(\tau), y, \varepsilon) - R_{\theta,+}(1, 0, y, \varepsilon)] \quad (12)$$

and

$$\phi_{\theta,-}(\tau, y, \varepsilon) = y + \varepsilon [R_{\theta,-}(\cos(\tau), \sin(\tau), y, \varepsilon) - R_{\theta,-}(1, 0, y, \varepsilon)] \quad (13)$$

where both $R_{\theta,+}$ and $R_{\theta,-}$ are modeled as MLPs. Additionally, the mappings $y \mapsto \phi_{\theta,+}(\tau, \cdot, \varepsilon) \circ \phi_{\theta,-}(\tau, \cdot, \varepsilon)(y)$ and $y \mapsto \phi_{\theta,-}(\tau, \cdot, \varepsilon) \circ \phi_{\theta,+}(\tau, \cdot, \varepsilon)(y)$ must closely approximate the identity to satisfy the auto-encoder structure [24]. Moreover, dependency w.r.t. τ with trigonometric functions comes from 2π -periodicity of ϕ^ε .

The complete numerical procedure consists of three main steps. First, data are collected by accurately simulating the exact flow at various points in the domain, requiring a large number of simulations and high precision to ensure a reliable approximation of the averaged field and high oscillation generator. Second, the neural networks are trained individually by minimizing a prescribed loss function to optimize their performance. Finally, given the initial data, an approximation of the exact solution is obtained by applying the same numerical scheme to the neural networks as was used during training.

- 1. Construction of the data set:** K "initial" data $y_0^{(k)}$ at time $t_0^{(k)}$ are randomly selected into a compact set $\Omega \subset \mathbb{R}^d$ (where we want to simulate the solution) with uniform distribution. The initial time $t_0^{(k)}$ is randomly chosen in $[0, 2\pi]$. Then, for all $0 \leq k \leq K-1$, we compute a very accurate approximation of the exact flow at times $h^{(k)}$ with initial condition $y_0^{(k)}$, denoted $y_1^{(k)}$. Step sizes $h^{(k)}$ and high oscillation parameters $\varepsilon^{(k)}$ are chosen in domains $[h_-, h_+]$ and $[\varepsilon_-, \varepsilon_+]$ respectively (we actually pick the values $\log h^{(k)}$ and $\log \varepsilon^{(k)}$ randomly in the domains $[\log h_-, \log h_+]$ and $[\log \varepsilon_-, \log \varepsilon_+]$ with uniform distribution).
- 2. Training the neural networks:** We minimize the Mean Squared Error (MSE), denoted $Loss_{Train}$, which measures the difference between the predicted data $\hat{y}_1^{(k)}$ and the "exact data"

²this map is invertible if ε is small enough, as a perturbation of the identity.

$y_1^{(k)}$, by computing the optimal parameters of the NN over K_0 data (where $1 \leq K_0 \leq K - 1$) using a gradient method:

$$\begin{aligned}
Loss_{Train} &= \frac{1}{K_0} \sum_{k=0}^{K_0-1} \underbrace{\left| \phi_{\theta,+} \left(\frac{t_0^{(k)} + h^{(k)}}{\varepsilon^{(k)}}, \cdot, \varepsilon^{(k)} \right) \circ \Phi_{h^{(k)}}^{F_\theta(\cdot, h^{(k)}, \varepsilon^{(k)})} \circ \phi_{\theta,-} \left(\frac{t_0^{(k)}}{\varepsilon^{(k)}}, \cdot, \varepsilon^{(k)} \right) (y_0^{(k)}) - \underbrace{\varphi_{h^{(k)}}^f(y_0^{(k)})}_{=y_1^{(k)}} \right|^2}_{=\hat{y}_1^{(k)}} \\
&+ \frac{1}{K_0} \sum_{k=0}^{K_0-1} \left| \phi_{\theta,+} \left(\frac{t_0^{(k)}}{\varepsilon^{(k)}}, \cdot, \varepsilon^{(k)} \right) \circ \phi_{\theta,-} \left(\frac{t_0^{(k)}}{\varepsilon^{(k)}}, \cdot, \varepsilon^{(k)} \right) (y_0^{(k)}) - y_0^{(k)} \right|^2 \\
&+ \frac{1}{K_0} \sum_{k=0}^{K_0-1} \left| \phi_{\theta,-} \left(\frac{t_0^{(k)}}{\varepsilon^{(k)}}, \cdot, \varepsilon^{(k)} \right) \circ \phi_{\theta,+} \left(\frac{t_0^{(k)}}{\varepsilon^{(k)}}, \cdot, \varepsilon^{(k)} \right) (y_0^{(k)}) - y_0^{(k)} \right|^2
\end{aligned} \tag{14}$$

The first term of $Loss_{Train}$ corresponds to the structure of the slow-fast decomposition equation, while the second and third terms correspond to the auto-encoder structure for the pair $(\phi_{\theta,+}, \phi_{\theta,-})$.

Simultaneously, we compute the value of another MSE, denoted as $Loss_{Test}$, which measures the difference between the predicted data $\hat{y}_1^{(k)}$ and the “exact data” $y_1^{(k)}$ for a subset of initial values that were not used during the training of the neural networks. The purpose of this step is to evaluate the performance of the training process on “unknown” initial values:

$$\begin{aligned}
Loss_{Test} &= \frac{1}{K - K_0} \sum_{k=K_0}^{K-1} \underbrace{\left| \phi_{\theta,+} \left(\frac{t_0^{(k)} + h^{(k)}}{\varepsilon^{(k)}}, \cdot, \varepsilon^{(k)} \right) \circ \Phi_{h^{(k)}}^{F_\theta(\cdot, h^{(k)}, \varepsilon^{(k)})} \circ \phi_{\theta,-} \left(\frac{t_0^{(k)}}{\varepsilon^{(k)}}, \cdot, \varepsilon^{(k)} \right) (y_0^{(k)}) - \hat{y}_1^{(k)} \right|^2}_{=\hat{y}_1^{(k)}} \\
&- \underbrace{\left| \varphi_{h^{(k)}}^f(y_0^{(k)}) \right|^2}_{=y_1^{(k)}} \\
&+ \frac{1}{K - K_0} \sum_{k=K_0}^{K-1} \left| \phi_{\theta,+} \left(\frac{t_0^{(k)}}{\varepsilon^{(k)}}, \cdot, \varepsilon^{(k)} \right) \circ \phi_{\theta,-} \left(\frac{t_0^{(k)}}{\varepsilon^{(k)}}, \cdot, \varepsilon^{(k)} \right) (y_0^{(k)}) - y_0^{(k)} \right|^2 \\
&+ \frac{1}{K - K_0} \sum_{k=K_0}^{K-1} \left| \phi_{\theta,-} \left(\frac{t_0^{(k)}}{\varepsilon^{(k)}}, \cdot, \varepsilon^{(k)} \right) \circ \phi_{\theta,+} \left(\frac{t_0^{(k)}}{\varepsilon^{(k)}}, \cdot, \varepsilon^{(k)} \right) (y_0^{(k)}) - y_0^{(k)} \right|^2
\end{aligned} \tag{15}$$

If $Loss_{Train}$ and $Loss_{Test}$ exhibit similar decay patterns, it indicates the absence of overfitting. In this case, the neural network model does not merely fit the training data but also maintains its ability to generalize and perform accurately on unknown data, which is its primary objective.

3. Numerical approximation using slow-fast decomposition: At the end of training process, an accurate approximation $F_\theta(\cdot, h, \varepsilon)$ of $\widehat{F_h^{\varepsilon, [n_\varepsilon], [q]}}$ is obtained. This approximation is then used to compute the successive values of $(\Phi_h^{\varepsilon, [n_\varepsilon]})^n(y_0)$ for $n = 0, \dots, N$. Additionally, an accurate approximation $\phi_{\theta,+}(\cdot, \cdot, \varepsilon)$ of ϕ^ε . As a result, an approximation of the solution can be visualized by plotting:

$$y_{\theta,n}^\varepsilon := \phi_{\theta,+} \left(\frac{t_n}{\varepsilon}, \left(\Phi_h^{F_\theta(\cdot, h, \varepsilon)} \right)^n (y_0), \varepsilon \right) \quad (16)$$

for all $n = 0, \dots, N$.

4. Numerical approximation using micro-macro correction: At the conclusion of the training, an alternative option is to reproduce the numerical integration using the Micro-Macro method by plotting:

$$y_{\theta,n}^\varepsilon = \phi_{\theta,+} \left(\frac{t_n}{\varepsilon}, v_{\theta,n}, \varepsilon \right) + w_{\theta,n}, \quad (17)$$

where, for all $n \in \mathbb{N}$:

$$v_{\theta,n} = \left(\Phi_h^{F_\theta(\cdot, h, \varepsilon)} \right)^n (y_0), \quad (18)$$

and

$$w_{\theta,n+1} = \left(\Phi_{t_n, h}^{g_\theta(\frac{t_n}{\varepsilon}, \cdot, v_{\theta,n}, \varepsilon)} \right) (w_{\theta,n}), \quad (19)$$

where, for all $(\tau, w, v, \varepsilon) \in [0, 2\pi] \times \Omega \times \Omega \times [0, 1]$,

$$g_\theta(\tau, w, v, \varepsilon) = f(\tau, \phi_{\theta,+}(\tau, v, \varepsilon) + w) - \frac{1}{\varepsilon} \partial_\tau \phi_{\theta,+}(\tau, v, \varepsilon) - \partial_y \phi_{\theta,+}(\tau, v, \varepsilon) F_\theta(v, 0, \varepsilon). \quad (20)$$

The micro-macro correction has the advantage of eliminating the need to learn the entire micro-macro vector field, which would require a dataset with double the dimensions and more data. Furthermore, this method does not necessitate more training than the *slow-fast* decomposition-based approach.

2.1.4 An alternative method for autonomous systems

Let us consider now autonomous highly oscillatory systems of the form

$$\dot{y}^\varepsilon(t) = \frac{1}{\varepsilon} A y^\varepsilon(t) + g(y^\varepsilon(t)), \quad (21)$$

where $A \in \mathcal{M}_d(\mathbb{R})$ be a matrix with eigenvalues in $i\mathbb{Z}$ and let $g : \mathbb{R}^d \rightarrow \mathbb{R}^d$ be a smooth function. A natural approach to analyze this system involves introducing the change of variables $z^\varepsilon(t) = e^{-\frac{t}{\varepsilon} A} y^\varepsilon(t)$ to get the new system

$$\dot{z}^\varepsilon(t) = e^{-\frac{t}{\varepsilon} A} g \left(e^{\frac{t}{\varepsilon} A} z^\varepsilon(t) \right), \quad (22)$$

which is a system of the form (1).

This system can also be studied directly in its autonomous form (21). A normal form theorem [13] guarantees the existence of a matrix A^ε and a vector field g^ε such that A^ε generates a periodic flow $\tau \mapsto \Phi_\tau^\varepsilon$, g^ε generates a flow $t \mapsto \varphi_t^{g^\varepsilon}$, the Lie bracket $[A^\varepsilon, g^\varepsilon]$ vanishes³. Moreover, for any $T > 0$, there exists a positive constant C_T such that for all $t \in [0, T]$ and $\varepsilon \in]0, 1]$, the following holds:

$$\left| y^\varepsilon(t) - \phi_{\frac{t}{\varepsilon}}^\varepsilon \left(\varphi_t^{g^\varepsilon}(y^\varepsilon(0)) \right) \right| \leq C_T e^{-\frac{C_T}{\varepsilon}}. \quad (23)$$

The main idea here is to approximate the flows Φ^ε and φ^{g^ε} using neural networks. This approach has the advantage of eliminating the need for an auto-encoder to learn ϕ^ε .

Specifically, we approximate $\varphi_h^{g^\varepsilon}$ with a neural network, denoted φ_θ modeled as an identity perturbation

$$\varphi_\theta(y, h, \varepsilon) = y + h R_{\theta, \varphi}(y, h, \varepsilon), \quad (24)$$

where $R_{\theta, \varphi}$ is a multilayer perceptron.

We also approximate the periodic flow $\tau \mapsto \Phi_\tau^\varepsilon$ using a neural network denoted ϕ_θ modeled as an identity perturbation:

$$\phi_\theta(\tau, y, \varepsilon) = y + [R_{\theta, \phi}(\cos(\tau), \sin(\tau), y, \varepsilon) - R_{\theta, \phi}(1, 0, y, \varepsilon)]. \quad (25)$$

where $R_{\theta, \phi}$ is also a multilayer perceptron. Structure of ϕ_θ follows structure of Φ^ε .

As in the classical case, the numerical procedure is divided into three main steps: data generation, training the neural networks through *loss* minimization, and numerical integration. Specifically, we adhere to the same methodology as in the classical case:

- 1. Data set construction:** We randomly select K initial conditions $y_0^{(k)}$ at time $t = 0$ from a compact set $\Omega \subset \mathbb{R}^d$ with a uniform distribution. Additionally, we randomly choose $h^{(k)} \in [h_-, h_+]$ and $\varepsilon^{(k)} \in [\varepsilon_-, \varepsilon_+]$ where $\log h^{(k)}$ and $\log \varepsilon^{(k)}$ are uniformly distributed. For each $0 \leq k \leq K - 1$, we compute $y_1^{(k)} = y^\varepsilon(h)$ using a highly accurate (and computationally expensive) integrator, providing a very precise approximation of the exact flow.
- 2. Training the neural networks:** We minimize the MSE loss function, $Loss_{Train}$ function, which quantifies the difference between the "exact" data and the predictions. This optimization is performed using a gradient-based method to find the optimal neural network parameters over K_0 data points:

³ A^ε can be considered as a linear vector field $y \mapsto A^\varepsilon y$. So we have $[A^\varepsilon, g^\varepsilon](y) = A^\varepsilon g^\varepsilon(y) - \partial_y g^\varepsilon(y) A^\varepsilon(y)$

$$\begin{aligned}
Loss_{Train} &:= \frac{1}{K_0} \sum_{k=0}^{K_0-1} \left| y_1^{(k)} - \phi_\theta \left(\frac{h^{(k)}}{\varepsilon^{(k)}}, \varphi_\theta(y_0^{(k)}, h^{(k)}, \varepsilon^{(k)}), \varepsilon^{(k)} \right) \right|^2 \\
&+ \frac{1}{K_0} \sum_{k=0}^{K_0-1} \left| \phi_\theta \left(\frac{h^{(k)}}{\varepsilon^{(k)}}, \varphi_\theta(y_0^{(k)}, h^{(k)}, \varepsilon^{(k)}), \varepsilon^{(k)} \right) \right. \\
&- \left. \varphi_\theta \left(\phi_\theta \left(\frac{h^{(k)}}{\varepsilon^{(k)}}, y_0^{(k)}, \varepsilon^{(k)} \right), h^{(k)}, \varepsilon^{(k)} \right) \right|^2. \tag{26}
\end{aligned}$$

The first term of $Loss_{Train}$ captures the structure of the equation involving both flows, while the second term enforces the property of flow commutativity, which is equivalent to the vanishing of the Lie bracket of the associated vector fields.

Simultaneously, we compute the MSE $Loss_{Test}$ to evaluate the performance of the training on "unknown" data:

$$\begin{aligned}
Loss_{Test} &:= \frac{1}{K - K_0} \sum_{k=K_0}^{K-1} \left| y_1^{(k)} - \phi_\theta \left(\frac{h^{(k)}}{\varepsilon^{(k)}}, \varphi_\theta(y_0^{(k)}, h^{(k)}, \varepsilon^{(k)}), \varepsilon^{(k)} \right) \right|^2 \\
&+ \frac{1}{K - K_0} \sum_{k=K_0}^{K-1} \left| \phi_\theta \left(\frac{h^{(k)}}{\varepsilon^{(k)}}, \varphi_\theta(y_0^{(k)}, h^{(k)}, \varepsilon^{(k)}), \varepsilon^{(k)} \right) \right. \\
&- \left. \varphi_\theta \left(\phi_\theta \left(\frac{h^{(k)}}{\varepsilon^{(k)}}, y_0^{(k)}, \varepsilon^{(k)} \right), h^{(k)}, \varepsilon^{(k)} \right) \right|^2. \tag{27}
\end{aligned}$$

3. Integration: At the end of the training, we obtain an accurate approximation of Φ^ε and φ^{g^ε} . We then plot the points $(y_{\theta,n}^\varepsilon)_{0 \leq n \leq N} = (\phi_\theta(\frac{t_n}{\varepsilon}, \varphi_\theta(\cdot, h, \varepsilon)^n(y^\varepsilon(0)), \varepsilon))_{0 \leq n \leq N}$ for $n = 0, \dots, N$.

2.2 Error analysis

In this subsection, we analyze the error arising from the methods described in the previous section. More specifically, we provide estimates of the global error for each of the standard numerical methods.

2.2.1 Slow-fast decomposition

The *slow-fast* decomposition offers a direct numerical method along with corresponding error bounds.

Theorem 1. *Let us denote the following learning errors:*

(i) **Learning error for high oscillation generator:**

$$\delta_{\phi,+} := \left\| \frac{\phi^{\varepsilon, [n_\varepsilon]} - \phi_{\theta,+}}{\varepsilon} \right\|_{L^\infty([0, 2\pi] \times \Omega \times [0, \varepsilon_+])} \tag{28}$$

(ii) *Learning error for modified averaged field:*

$$\delta_F := \left\| \widetilde{F_h^{\varepsilon, [n_\varepsilon], [q]}} - F_\theta \right\|_{L^\infty(\Omega \times [0, h_+] \times [0, \varepsilon_+])}, \quad (29)$$

Let us consider these two hypotheses:

(i) For $f_1, f_2 : \Omega \rightarrow \mathbb{R}^d$ smooth enough, we have, for all $h > 0$,

$$\left\| \Phi_h^{f_1} - \Phi_h^{f_2} \right\|_{L^\infty(\Omega)} \leq C h \|f_1 - f_2\|_{L^\infty(\Omega)} \quad (30)$$

for some positive constant $C > 0$ independent on f_1 and f_2 .

(ii) For $f : \Omega \rightarrow \mathbb{R}^d$ sufficiently smooth, there exists $L_f > 0$ s.t. for all $y_1, y_2 \in \Omega$ and for all $h > 0$, we have

$$\left| \Phi_h^f(y_1) - \Phi_h^f(y_2) \right| \leq (1 + L_f h) |y_1 - y_2| \quad (31)$$

Let $y_{\theta, n}^\varepsilon$ denote the following numerical flow:

$$y_{\theta, n}^\varepsilon := \phi_{\theta, +} \left(\frac{t_n}{\varepsilon}, \left(\Phi_h^{F_\theta(\cdot, h, \varepsilon)} \right)^n (y_0), \varepsilon \right). \quad (32)$$

Then there exist constants $\lambda, \alpha > 0$ (independent of h, ε) s.t. for all $h \leq h_+$ and $\varepsilon \in]0, \varepsilon_0]$,

$$|y^\varepsilon(t_n) - y_{\theta, n}^\varepsilon| \leq M e^{-\frac{\beta \varepsilon_0}{\varepsilon}} + \delta_{\phi, +} \varepsilon + (1 + \alpha \varepsilon) \frac{e^{\lambda T} - 1}{\lambda} \left[\bar{C} h^{p+q-1} + C \delta_F \right]. \quad (33)$$

Remarks. (i) The vector fields $\phi^{\varepsilon, [n_\varepsilon]}$ and $\widetilde{F_h^{\varepsilon, [n_\varepsilon]}}$ are smooth by construction, as shown in the formulas (52) and (53)). Similarly, $\phi_{\theta, -}$, $\phi_{\theta, +}$ and F_θ are also smooth because they result from the composition of affine function A_1, \dots, A_{L+1} and nonlinear activation functions $\sigma_1, \dots, \sigma_L$. For L layers, the output of the neural network takes the form $A_{L+1} \circ \Sigma_L \circ A_L \circ \dots \circ \Sigma_1 \circ A_1$. Therefore, if the activation functions are smooth, so are $\phi_{\theta, -}$, $\phi_{\theta, +}$, and F_θ . This is the case, for example, when the Σ_i 's are hyperbolic tangent functions.

(ii) A similar error estimate holds for a variable step-size implementation of the numerical method Φ : if we use the step sequence $0 \leq h_j \leq h_+$, then $T = h_0 + \dots + h_{N-1}$, $t_n = h_0 + \dots + h_{n-1}$ and

$$y_{\theta, n} = \phi_{\theta, +} \left(\frac{t_n}{\varepsilon}, \Phi_{h_{n-1}}^{F_\theta(\cdot, h_{n-1}, \varepsilon)} \circ \dots \circ \Phi_{h_0}^{F_\theta(\cdot, h_0, \varepsilon)} (y^\varepsilon(0)), \varepsilon \right) \quad (34)$$

where constants $\lambda, \alpha > 0$ (independent of h, ε) s.t. for all $h \leq h_+$ and $\varepsilon \in]0, 1]$:

$$\max_{0 \leq n \leq N} |y^\varepsilon(t_n) - y_{\theta, n}| \leq M e^{-\frac{\beta \varepsilon_0}{\varepsilon}} + \delta_{\phi, +} \varepsilon + (1 + \alpha \varepsilon) \frac{e^{\lambda T} - 1}{\lambda} \left[\bar{C} h^{p+q-1} + C \delta_F \right]. \quad (35)$$

2.2.2 Micro-Macro correction

By applying the method of *slow-fast* decomposition to derive a numerical technique based on micro-macro decomposition, we obtain a novel numerical method along with its corresponding error bounds for numerical approximation.

Theorem 2. *Let us consider $p \in \mathbb{N}^*$ and denote the following learning errors:*

(i) *Learning error for high oscillation generator:*

$$\delta_{\phi,+} := \left\| \frac{\phi^{[p]} - \phi_{\theta,+}}{\varepsilon} \right\|_{W^{1,\infty}(\Omega \times [0,2\pi]), L^\infty([0,\varepsilon_+])} \quad (36)$$

(ii) *Learning error for modified averaged field:*

$$\delta_F := \left\| \widetilde{F_h^{[p],[q]}} - F_\theta \right\|_{L^\infty([0,2\pi] \times [0,\varepsilon_+])} \quad (37)$$

(iii) *Learning error for field of associated to micro part:*

$$\delta_g := \|g - g_\theta\|_{L^\infty([0,2\pi] \times \Omega \times \Omega \times [0,\varepsilon_+])} \quad (38)$$

Let $\Phi_{t,h}$ denote a numerical method of order p (depending on time t). Consider the following two hypotheses:

(i) For $f_1, f_2 : [0, T] \times \Omega \rightarrow \mathbb{R}^d$ sufficiently smooth and $t \in [0, T]$, we have, for all $h > 0$,

$$\left\| \Phi_{t,h}^{f_1} - \Phi_{t,h}^{f_2} \right\|_{L^\infty(\Omega)} \leq C h \|f_1 - f_2\|_{L^\infty(\Omega)} \quad (39)$$

for some positive constant $C > 0$ independent of f_1 and f_2 .

(ii) For $f : [0, T] \times \Omega \rightarrow \mathbb{R}^d$ sufficiently smooth and $t \in [0, T]$, there exists $L_f > 0$ s.t. for all $y_1, y_2 \in \Omega$ and for all $h > 0$, we have

$$\left| \Phi_{t,h}^f(y_1) - \Phi_{t,h}^f(y_2) \right| \leq (1 + L_f h) |y_1 - y_2| \quad (40)$$

Then, there exist constants $\alpha_\phi, \lambda, \mu, M, \beta > 0$ (independent of h, ε) s.t. for all $h \leq h_+$ and $\varepsilon \in]0, 1]$:

$$\begin{aligned} \max_{0 \leq n \leq N} |y^\varepsilon(t_n) - y_{\theta,n}^\varepsilon| &\leq \delta_{\phi,+} \varepsilon + \alpha_\phi \frac{e^{\lambda T} - 1}{\lambda} \left[\bar{C} h^{p+q-1} + C \delta_F \right] \\ &+ \frac{e^{\mu T} - 1}{\mu} \left[M' h^p + \frac{e^{\lambda T} - 1}{\lambda} \beta (\bar{C} h^{p+q-1} + C \delta_F) + C \delta_g \right] \end{aligned} \quad (41)$$

Remarks. (i) For some nonnegative constants $L_f, \alpha_{\theta,F}$ and α_ϕ independent of h, ε , we get:

$$\delta_g \leq (1 + L_f + \alpha_{\theta,F}\varepsilon)\delta_\phi + \alpha_\phi\delta_F \quad (42)$$

- (ii) Although the flow can be considered for non-autonomous differential equations and depends on time, the previous estimates concerning the numerical flow are assumed to be independent of time (except for the integration time T).
- (iii) The norm $\|\cdot\|_{W^{1,\infty}(\Omega \times [0,2\pi]), L^\infty([0,\varepsilon_+])}$ corresponds to $W^{1,\infty}$ -Sobolev norm w.r.t. the variables y and τ and L^∞ -norm w.r.t. the variable ε .

2.2.3 Alternative method

Alternative method for autonomous case yields to specific numerical error bounds.

Theorem 3. Let consider and denote the following learning errors:

(i) Learning error for flow ϕ^ε (high oscillations):

$$\delta_\Phi := \underset{(\tau,y,\varepsilon) \in [0,2\pi] \times \Omega \times [0,\varepsilon_+]}{\text{Max}} |\Phi_\tau^\varepsilon(y) - \phi_\theta(\tau, y, \varepsilon)|. \quad (43)$$

(ii) Learning error for flow φ^{g^ε} :

$$\delta_\varphi := \underset{(y,h,\varepsilon) \in \Omega \times [0,h_+] \times [0,\varepsilon_+]}{\text{Max}} \left| \frac{\varphi_h^{g^\varepsilon}(y) - \varphi_\theta(y, h, \varepsilon)}{h} \right|. \quad (44)$$

Then there exist positive constants λ, L and C_T such that, for all $\varepsilon \in]0, 1]$:

$$\underset{0 \leq n \leq N}{\text{Max}} |y_{\theta,n}^\varepsilon - y^\varepsilon(t_n)| \leq \delta_\Phi + L \frac{e^{\lambda_\theta T} - 1}{\lambda} \delta_\varphi + C_T e^{-\frac{C_T}{\varepsilon}} \quad (45)$$

3 Numerical experiments

To illustrate our theoretical results, we tested the method outlined in subsection 2.1 on a simple dynamical system from physics:

1. Inverted Pendulum: This dynamical system describes the evolution of an unstable pendulum, with its center of gravity above the pivot point, undergoing forced oscillations. It is governed by the following equation:

$$\begin{cases} \dot{y}_1^\varepsilon(t) &= y_2^\varepsilon(t) + \sin\left(\frac{t}{\varepsilon}\right) \sin(y_1^\varepsilon(t)) \\ \dot{y}_2^\varepsilon(t) &= \sin(y_1^\varepsilon(t)) - \frac{1}{2} \sin\left(\frac{t}{\varepsilon}\right)^2 \sin(2y_1^\varepsilon(t)) - \sin\left(\frac{t}{\varepsilon}\right) \cos(y_1^\varepsilon(t)) y_2^\varepsilon(t) \end{cases} \quad (46)$$

and the average field associated to this equation is given by

$$\langle f \rangle(y) = \begin{bmatrix} y_2 \\ \sin(y_1) - \frac{1}{4} \sin(2y_1) \end{bmatrix} \quad (47)$$

2. Van der Pol oscillator: This system models an electrical circuit with nonlinear damping. It is governed by the following two-dimensional system:

$$\begin{cases} \dot{q} &= \frac{1}{\varepsilon} p \\ \dot{p} &= -\frac{1}{\varepsilon} q + \left(\frac{1}{4} - q^2\right) p \end{cases} \quad (48)$$

by performing the variable change $(y_1, y_2) \mapsto S\left(\frac{t}{\varepsilon}\right)(q, p)$, where $\tau \mapsto S(\tau)$ is given by

$$\tau \mapsto S(\tau) = \begin{bmatrix} \cos(\tau) & -\sin(\tau) \\ \sin(\tau) & \cos(\tau) \end{bmatrix} \quad (49)$$

we get the system:

$$\begin{cases} \dot{y}_1(t) &= -\sin\left(\frac{t}{\varepsilon}\right) \left[\frac{1}{4} - (y_1(t) \cos\left(\frac{t}{\varepsilon}\right) + y_2(t) \sin\left(\frac{t}{\varepsilon}\right))^2 \right] \left[-y_1(t) \sin\left(\frac{t}{\varepsilon}\right) + y_2(t) \cos\left(\frac{t}{\varepsilon}\right) \right] \\ \dot{y}_2(t) &= \cos\left(\frac{t}{\varepsilon}\right) \left[\frac{1}{4} - (y_1(t) \cos\left(\frac{t}{\varepsilon}\right) + y_2(t) \sin\left(\frac{t}{\varepsilon}\right))^2 \right] \left[-y_1(t) \sin\left(\frac{t}{\varepsilon}\right) + y_2(t) \cos\left(\frac{t}{\varepsilon}\right) \right] \end{cases} \quad (50)$$

which is the classical form for highly oscillatory systems. The average field of the system in its canonical form is given, for all $y \in \mathbb{R}^2$, by

$$\langle f \rangle(y) = \frac{1}{8}(1 - |y|^2)y. \quad (51)$$

For a highly oscillatory differential equation of the form (1), one can approximate the averaged field F^ε and the highly oscillatory generator ϕ^ε (defined by the formal power series (3)) using the following approximation sequences [14]:

$$\begin{cases} \phi_\tau^{[0]}(y) &= y \\ \phi_\tau^{[k+1]}(y) &= y + \varepsilon \int_0^\tau f\left(\sigma, \phi_\sigma^{[k]}(y)\right) - \frac{\partial \phi_\sigma^{[k]}}{\partial y}(y) F^{[k]}(y) d\sigma \end{cases} \quad (52)$$

and

$$\begin{cases} F^{[0]}(y) &= \langle f \rangle(y) \\ F^{[k]}(y) &= \left(\frac{\partial \langle \phi^{[k]} \rangle}{\partial y}(y)\right)^{-1} \left\langle f\left(\cdot, \phi_\cdot^{[k]}(y)\right) \right\rangle. \end{cases} \quad (53)$$

These sequences can be used to obtain an approximation of arbitrary order for the formal power series (3)

$$\phi_\tau^\varepsilon(y) = \phi_\tau^{[k]}(y) + O\left(\varepsilon^{k+1}\right) \text{ and } F^\varepsilon(y) = F^{[k]}(y) + O\left(\varepsilon^{k+1}\right) \quad (54)$$

3.1 Approximation of the averaged field and high oscillation generator

In this subsection, we investigate the approximation error between the learned averaged field and the high-oscillation generator, compared to the theoretical averaged field and the high-oscillation generator, both at orders 0 and 1 for the inverted pendulum. We examine the learning error with respect to the high-oscillation parameter ε . Specifically, we compute the values

$$\max_{y \in \Omega} |F_\theta(y, 0, \varepsilon) - F^{[k]}(y)| \text{ and } \max_{(\tau, y) \in [0, 2\pi] \times \Omega} |\phi_{\theta,+}(\tau, y, \varepsilon) - \phi_\tau^{[k]}(y)| \quad (55)$$

where $\phi^{[k]}$ and $F^{[k]}$ are computed using the formulas (52) and (53) for $k = 0, 1$ respectively.

The figures 1, 2 and 3 confirm that the modified field can be effectively learned with our neural network. However, the learning error seems to slow the decay of the error bounds.

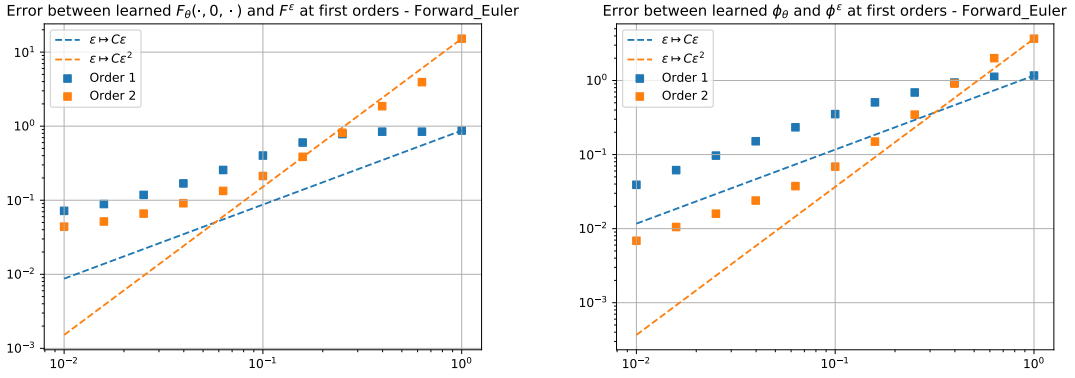


Figure 1: Inverted pendulum with forward Euler method. Left: Error between $F^{[k]}$ and $F_\theta(\cdot, 0, \varepsilon)$ for $k = 0, 1$ w.r.t. ε . Right: Error between $\phi^{[k]}$ and $\phi_{\theta,+}(\cdot, \cdot, \varepsilon)$ for $k = 0, 1$ w.r.t. ε .



Figure 2: Inverted pendulum with midpoint method. Left: Error between $F^{[k]}$ and $F_\theta(\cdot, 0, \varepsilon)$ for $k = 0, 1$ w.r.t. ε . Right: Error between $\phi^{[k]}$ and $\phi_{\theta,+}(\cdot, \cdot, \varepsilon)$ for $k = 0, 1$ w.r.t. ε .

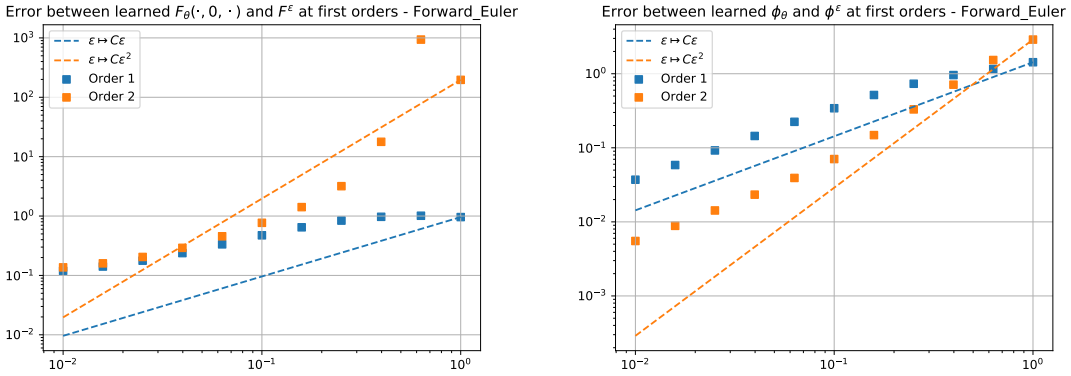


Figure 3: Van der Pol oscillator with forward Euler method. Left: Error between $F^{[k]}$ and $F_\theta(\cdot, 0, \varepsilon)$ for $k = 0, 1$ w.r.t. ε . Right: Error between $\phi^{[k]}$ and $\phi_{\theta,+}(\cdot, \cdot, \varepsilon)$ for $k = 0, 1$ w.r.t. ε .

3.2 Loss decay and integration of ODE's

To compare the integration of a dynamical system using the learned modified averaged field and the learned high-oscillation generator, we will solve the inverted pendulum problem using the Forward Euler and Midpoint methods. Before doing so, we examine the decay of the loss functions for the training and test data sets ($Loss_{Train}$ and $Loss_{Test}$). Their similarity provides a good indication that there is no overfitting, suggesting that the size of the training data set has been appropriately estimated. Since the MSE loss is used, it offers an insight into the square of the error for both the equation and the auto-encoder structure.

Figures 4, 5, 8, and 9 demonstrate accurate numerical integration using the slow-fast decomposition-based method, applying the corresponding learned vector field for both the Forward Euler and Midpoint methods for the inverted pendulum. For the Van der Pol oscillator, although the learning for the transformed dynamical system appears to be less accurate (figures 12 and 14), the integration after the inverse variable change (49) appears to be correct, as shown in figures 13 and 15.

However, incorporating the micro-macro correction significantly enhances the accuracy, especially for larger values of ε . In particular, the numerical approximation of the solution for the inverted pendulum becomes more accurate, as observed in figures 6, 7, 10, and 11. For the Van der Pol oscillator, it can be seen that the system's solution is accurately approximated using the micro-macro correction, as shown in figures 16 and 18, even before the variable change, as can be seen in figures 17 and 19.

3.2.1 Inverted Pendulum - forward Euler method

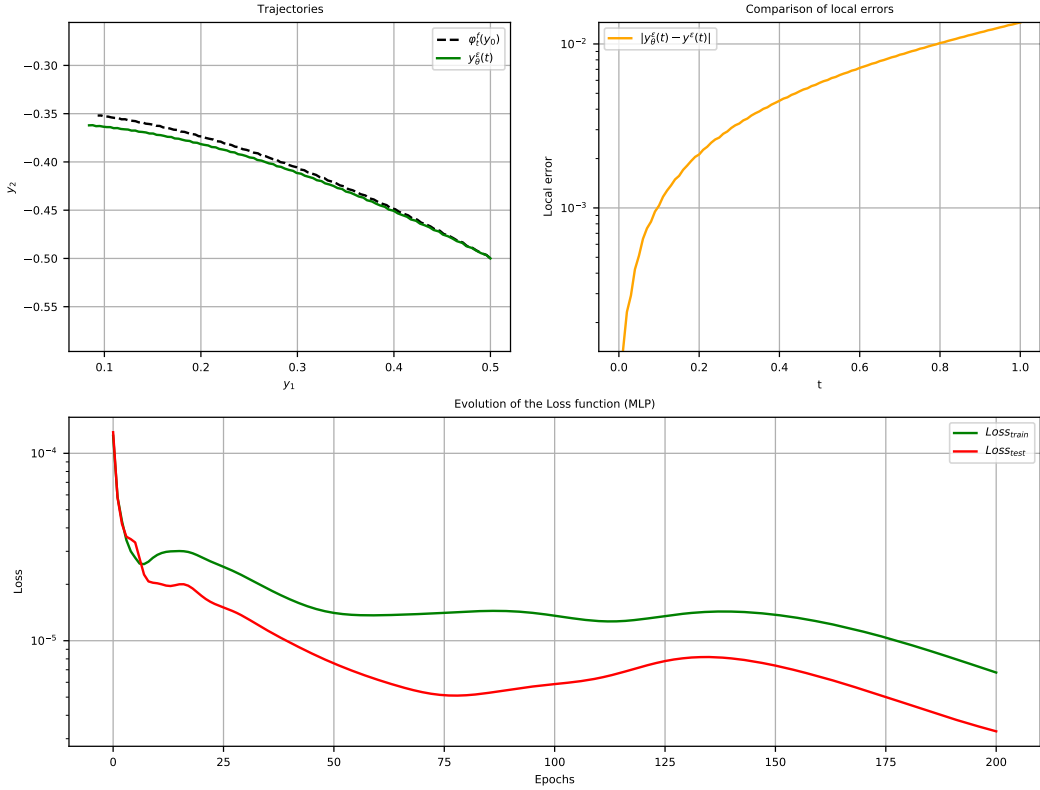


Figure 4: Comparison between *Loss* decays (green: $LOSS_{Train}$, red: $LOSS_{Test}$), trajectories (dashed dark: exact flow, green: numerical flow with learned vector fields and local error (yellow) for the inverted pendulum with Forward Euler method in the case $\varepsilon = 0.001$.

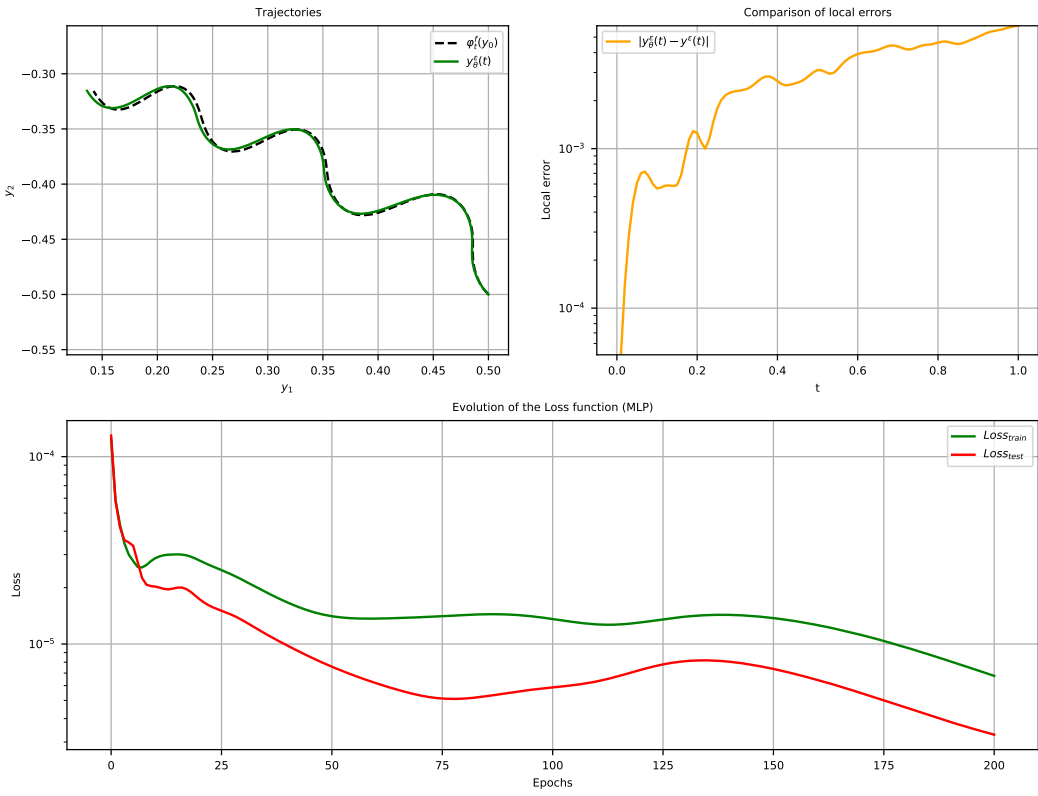


Figure 5: Comparison between *Loss* decays (green: $Loss_{Train}$, red: $Loss_{Test}$), trajectories (dashed dark: exact flow, green: numerical flow with learned vector fields and local error (yellow) for the inverted pendulum with Forward Euler method in the case $\varepsilon = 0.05$.

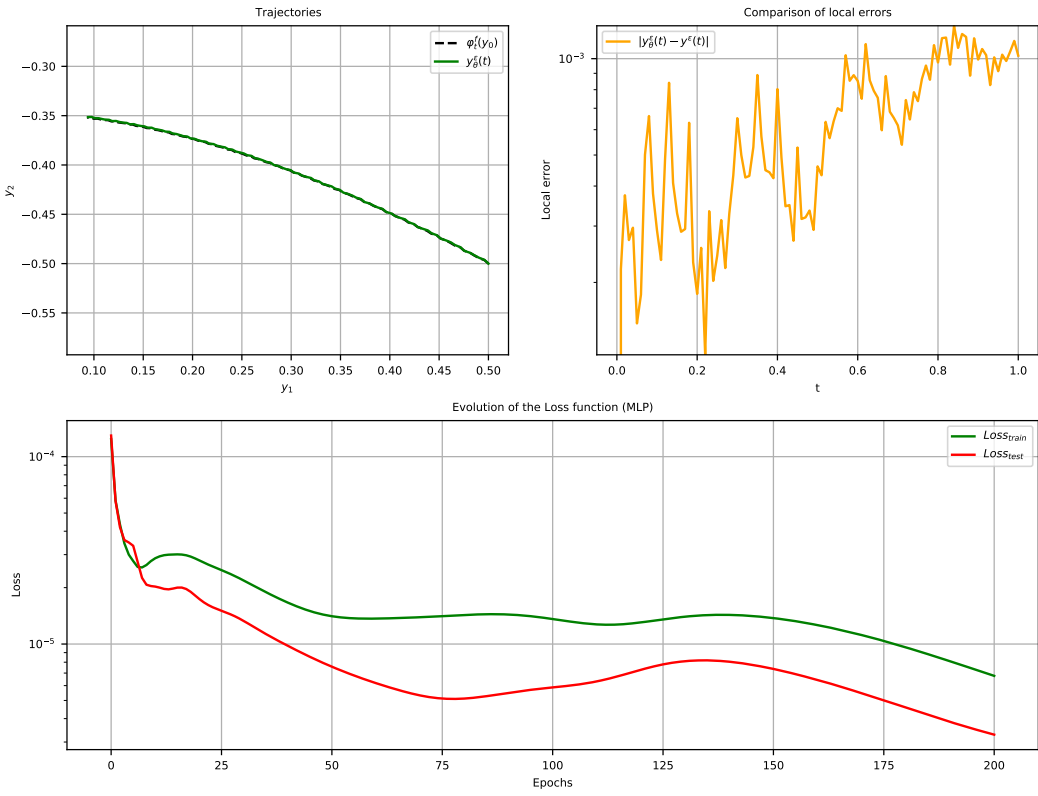


Figure 6: Comparison between *Loss* decays (green: $Loss_{Train}$, red: $Loss_{Test}$), trajectories (dashed dark: exact flow, green: numerical flow with learned vector fields and local error (yellow) for the inverted pendulum with Forward Euler method with Micro-Macro correction in the case $\varepsilon = 0.001$.

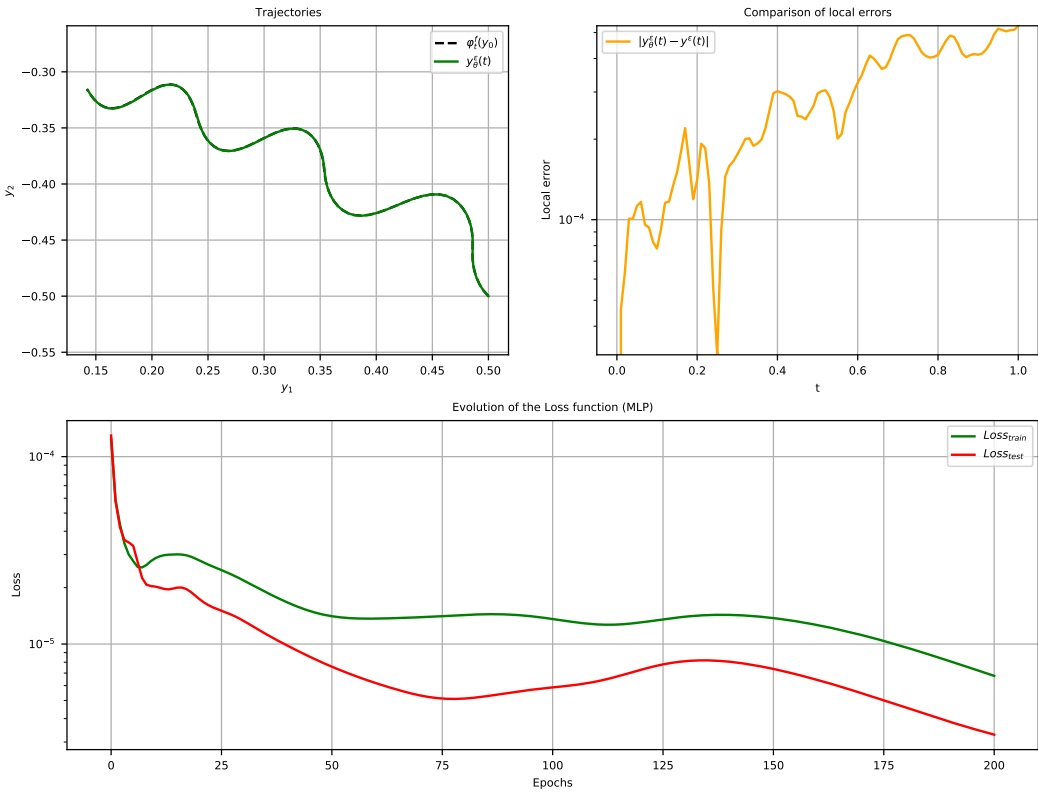


Figure 7: Comparison between *Loss* decays (green: $Loss_{Train}$, red: $Loss_{Test}$), trajectories (dashed dark: exact flow, green: numerical flow with learned vector fields and local error (yellow) for the inverted pendulum with Forward Euler method with Micro-Macro correction in the case $\varepsilon = 0.05$.

3.2.2 Inverted Pendulum - midpoint method

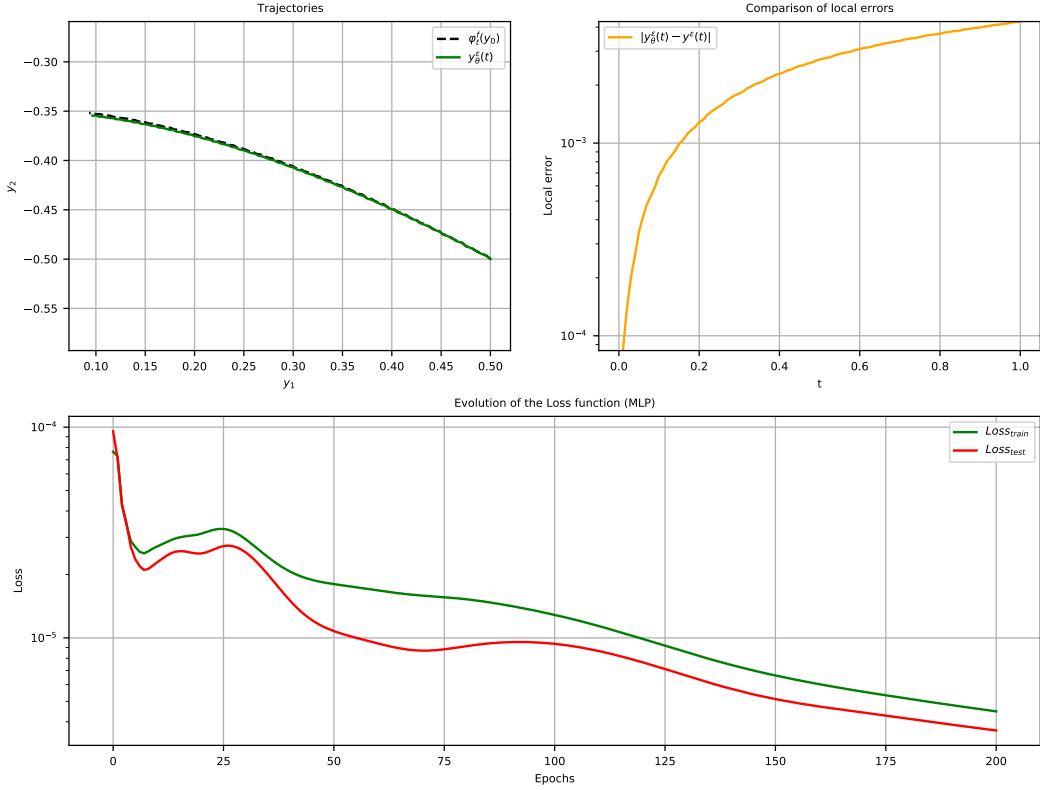


Figure 8: Comparison between *Loss* decays (green: $Loss_{Train}$, red: $Loss_{Test}$), trajectories (dashed dark: exact flow, green: numerical flow with learned vector fields and local error (yellow) for the inverted pendulum with midpoint method in the case $\varepsilon = 0.001$.

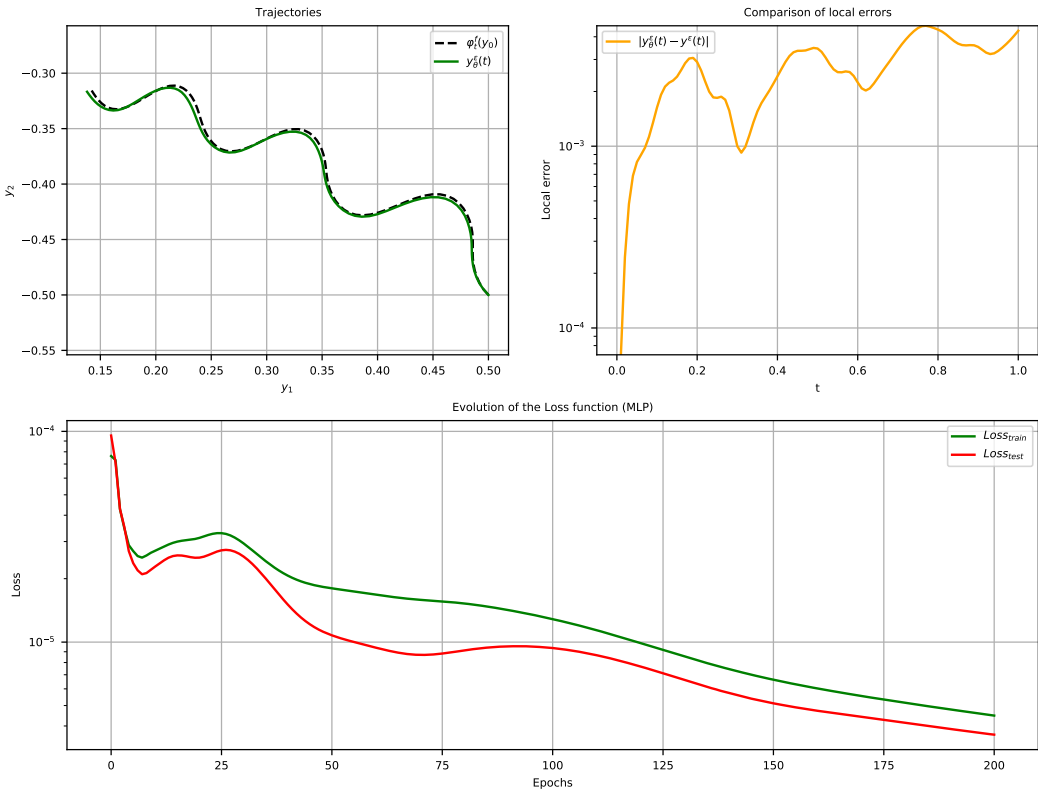


Figure 9: Comparison between *Loss* decays (green: $Loss_{Train}$, red: $Loss_{Test}$), trajectories (dashed dark: exact flow, green: numerical flow with learned vector fields and local error (yellow) for the inverted pendulum with midpoint method in the case $\varepsilon = 0.05$.

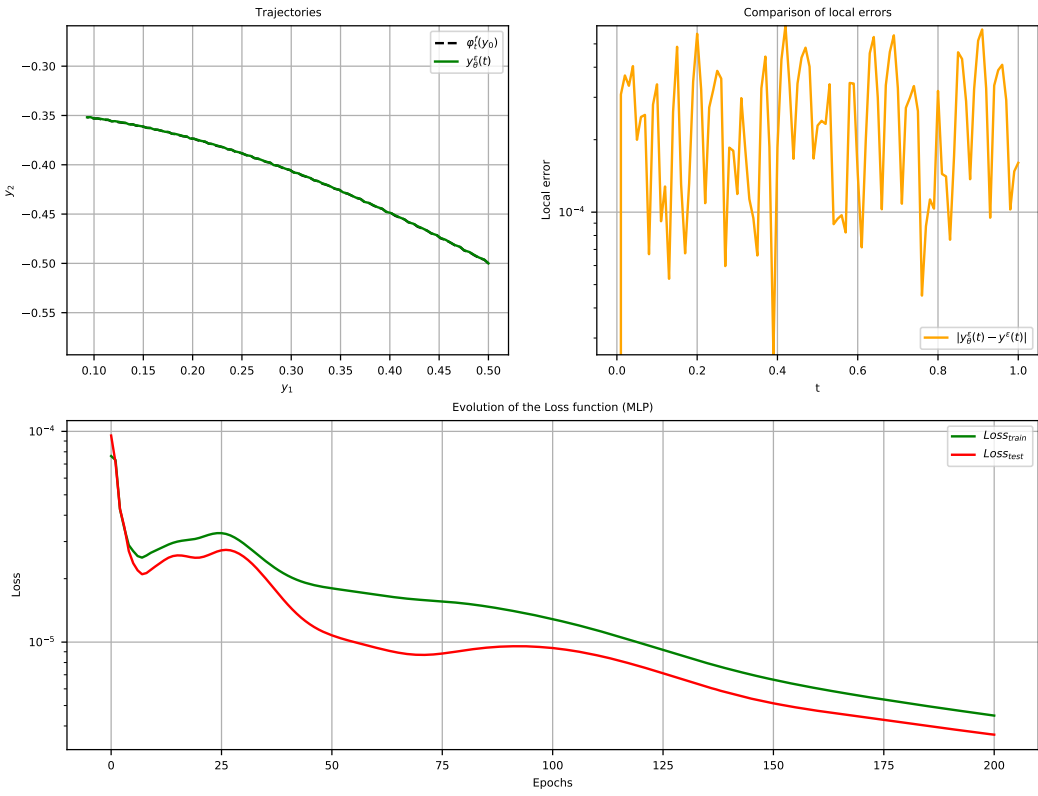


Figure 10: Comparison between *Loss* decays (green: $Loss_{Train}$, red: $Loss_{Test}$), trajectories (dashed dark: exact flow, green: numerical flow with learned vector fields and local error (yellow) for the inverted pendulum with midpoint method with Micro-Macro correction in the case $\varepsilon = 0.001$.

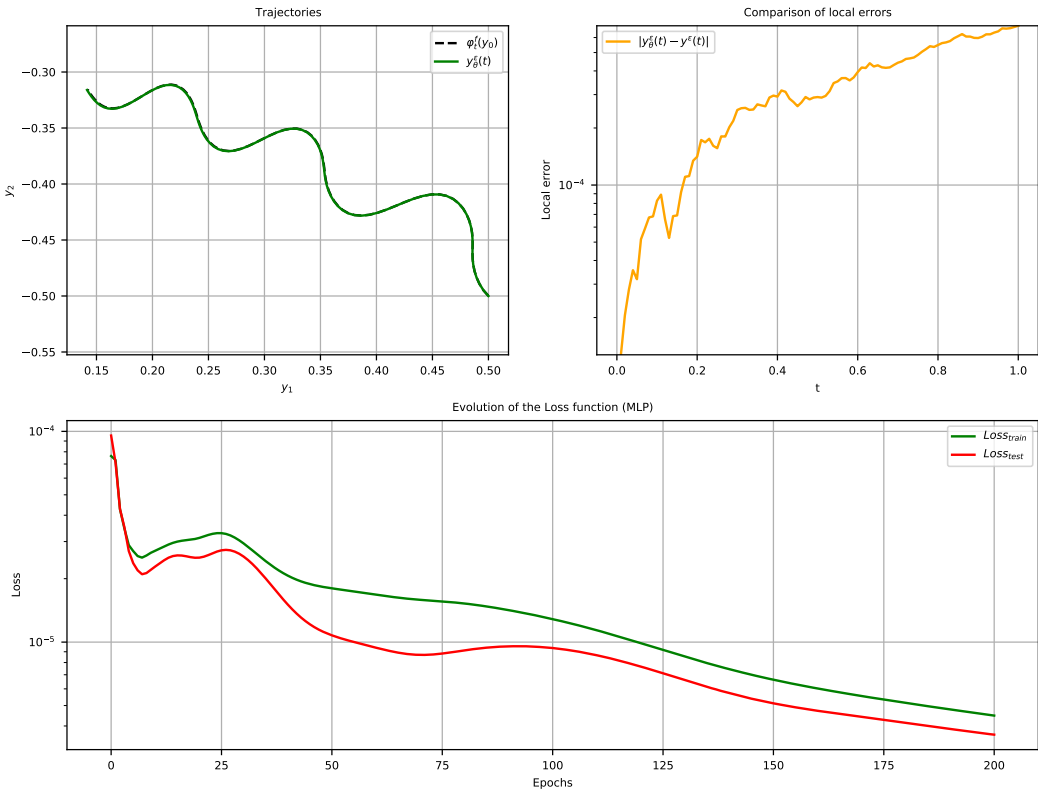


Figure 11: Comparison between *Loss* decays (green: $Loss_{Train}$, red: $Loss_{Test}$), trajectories (dashed dark: exact flow, green: numerical flow with learned vector fields and local error (yellow) for the inverted pendulum with midpoint method with Micro-Macro correction in the case $\varepsilon = 0.05$.

3.2.3 Van der Pol oscillator - forward Euler method

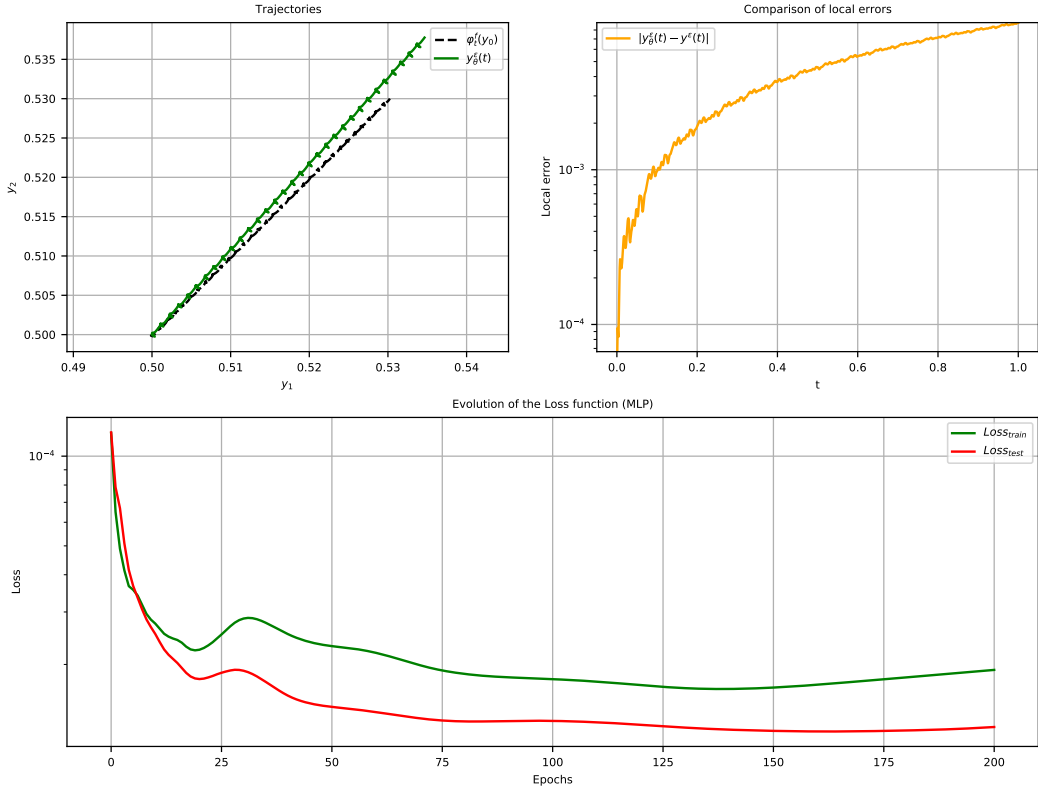


Figure 12: Comparison between *Loss* decays (green: $Loss_{Train}$, red: $Loss_{Test}$), trajectories (dashed dark: exact flow, green: numerical flow with learned vector fields and local error (yellow) for the Van der Pol oscillator with Forward Euler method in the case $\varepsilon = 0.01$.

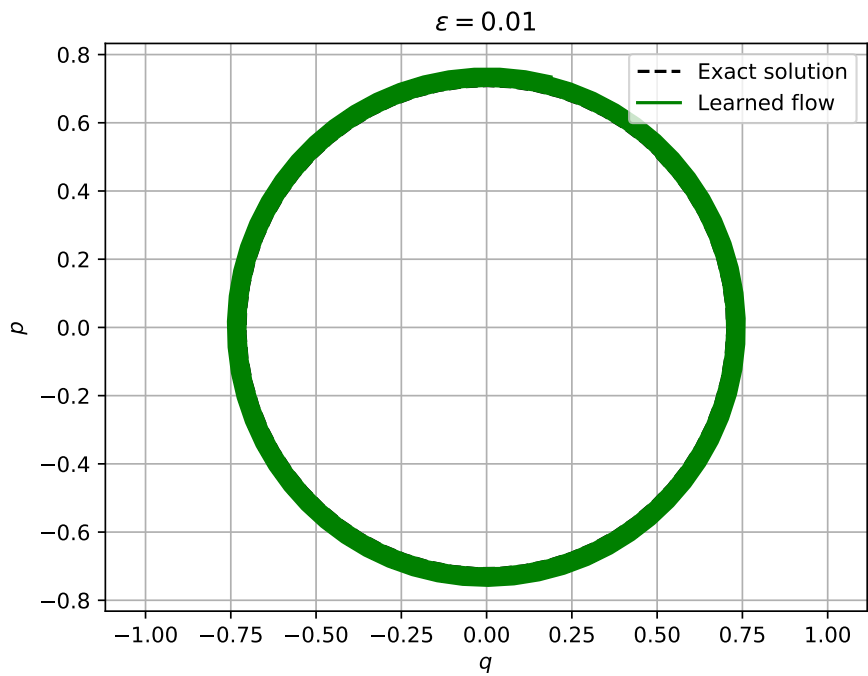


Figure 13: Comparison between trajectories (dashed dark: exact flow, green: numerical flow with learned vector field) for the Van der Pol oscillator with Forward Euler method in the case $\varepsilon = 0.01$ after the inverse variable change (49).

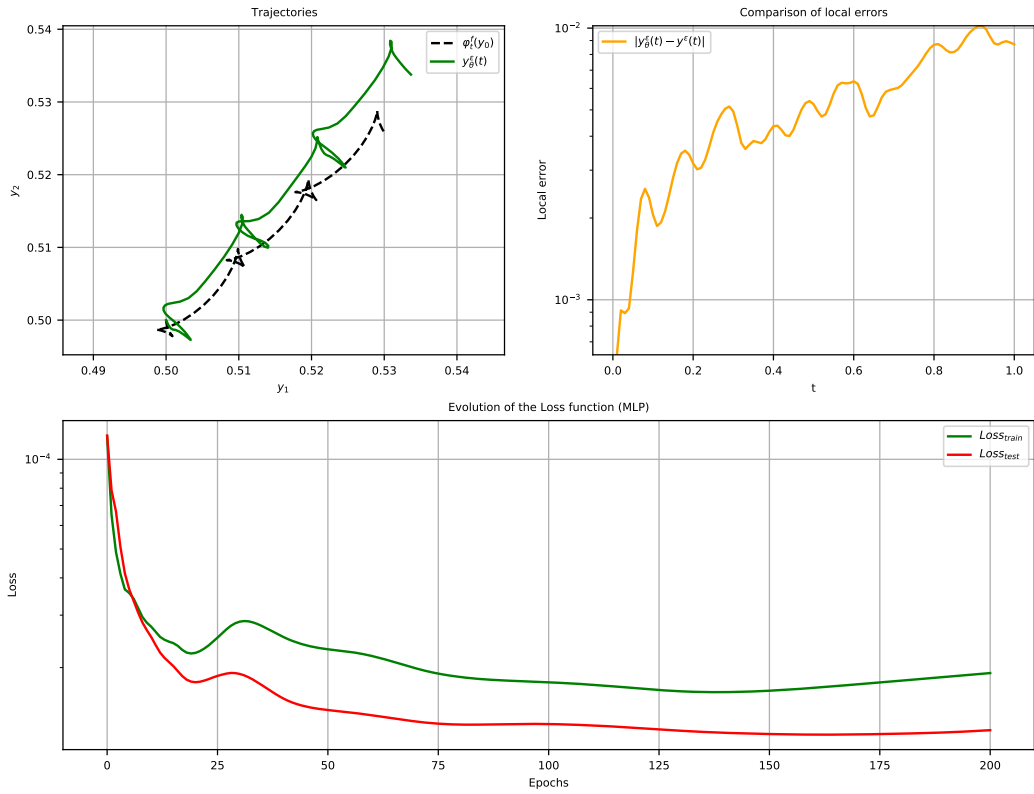


Figure 14: Comparison between *Loss* decays (green: $Loss_{Train}$, red: $Loss_{Test}$), trajectories (dashed dark: exact flow, green: numerical flow with learned vector fields and local error (yellow) for the Van der Pol oscillator with Forward Euler method in the case $\varepsilon = 0.1$.

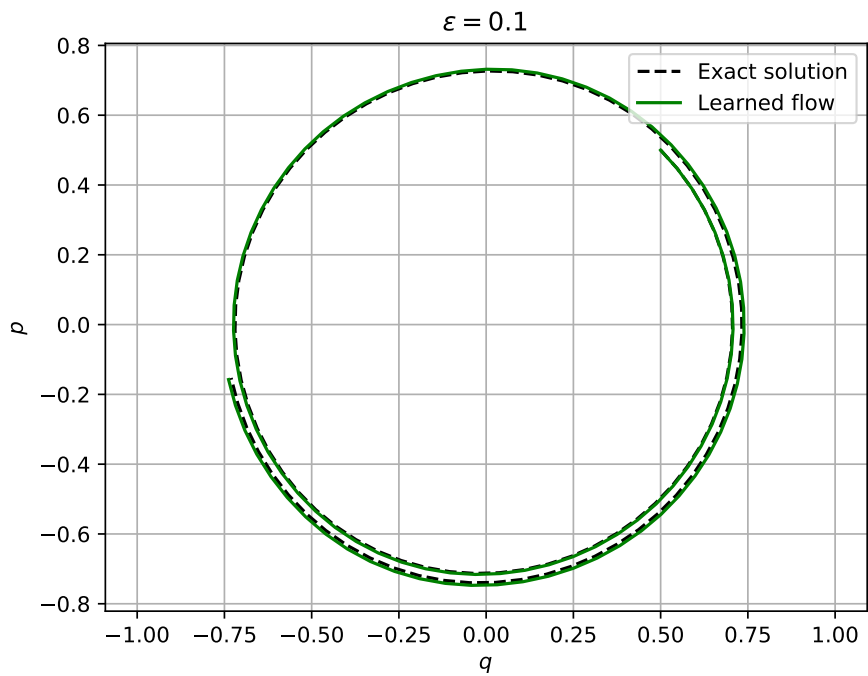


Figure 15: Comparison between trajectories (dashed dark: exact flow, green: numerical flow with learned vector field) for the Van der Pol oscillator with Forward Euler method in the case $\varepsilon = 0.1$ after the inverse variable change (49).

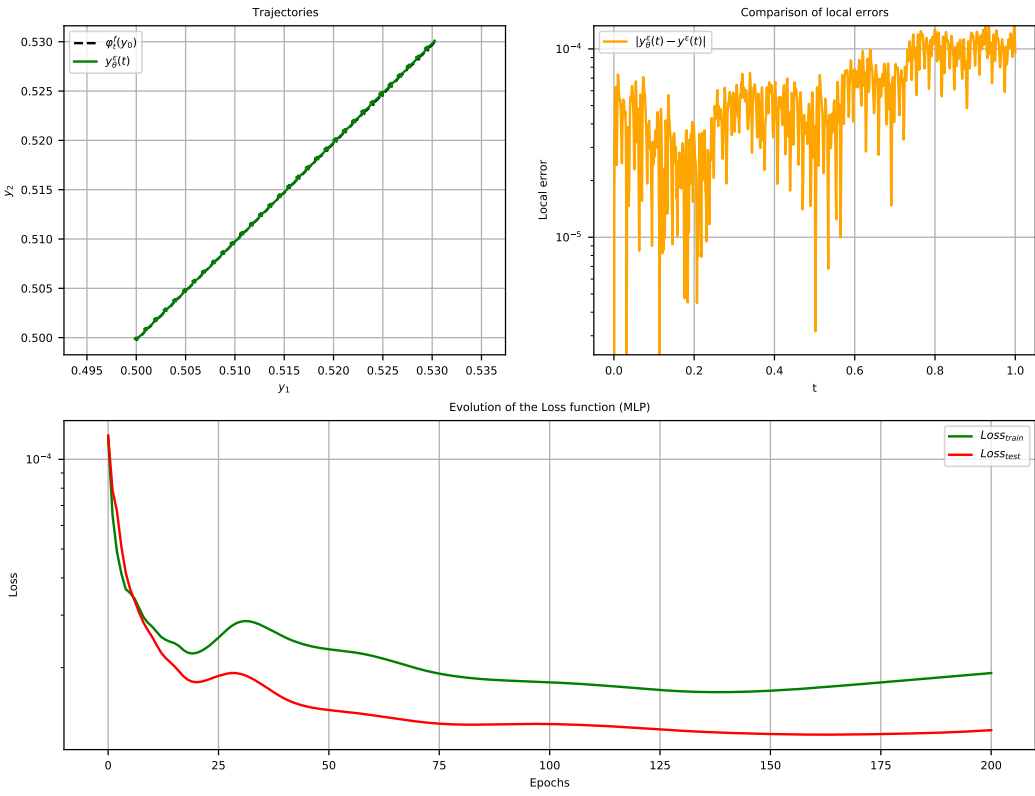


Figure 16: Comparison between *Loss* decays (green: $Loss_{Train}$, red: $Loss_{Test}$), trajectories (dashed dark: exact flow, green: numerical flow with learned vector fields and local error (yellow) for the Van der Pol oscillator with Forward Euler method with Micro-Macro correction in the case $\varepsilon = 0.01$.

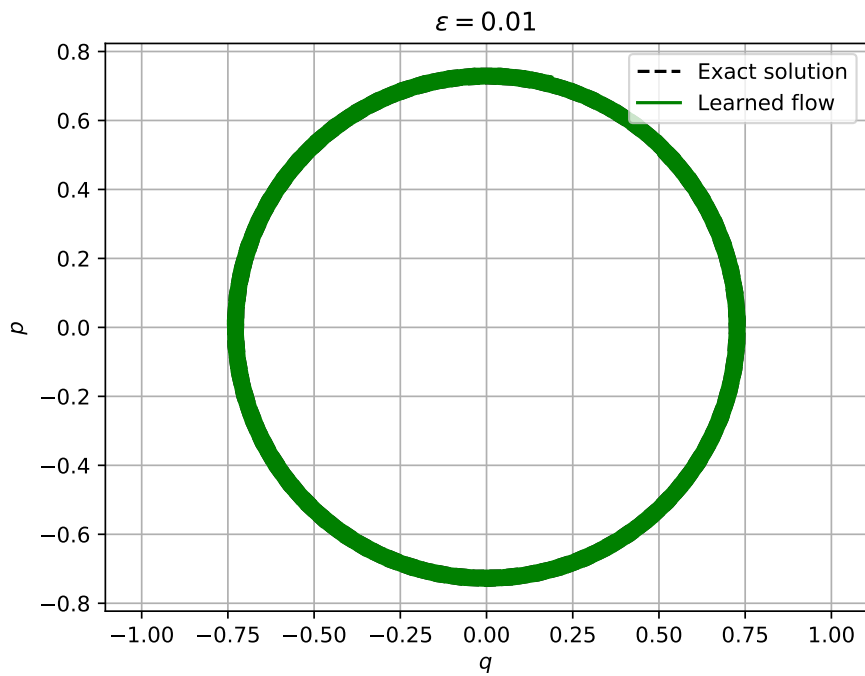


Figure 17: Comparison between trajectories (dashed dark: exact flow, green: numerical flow with learned vector field) for the Van der Pol oscillator with Forward Euler method with Micro-Macro correction in the case $\varepsilon = 0.01$ after the inverse variable change (49).

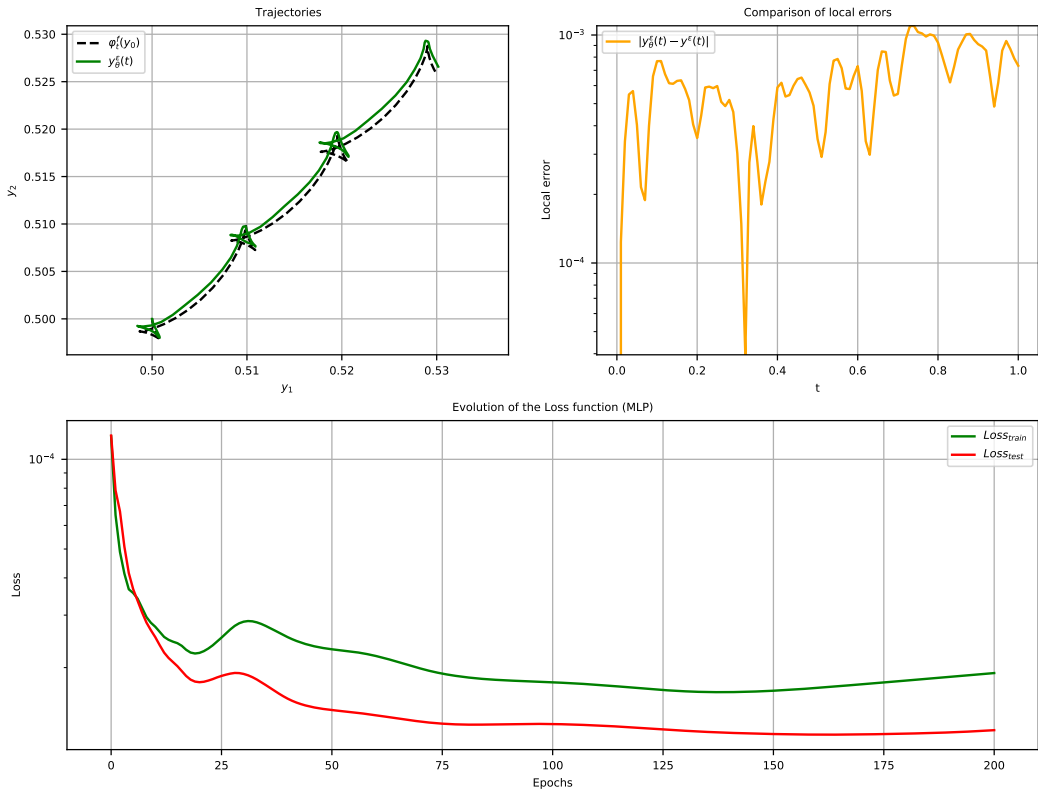


Figure 18: Comparison between *Loss* decays (green: $Loss_{Train}$, red: $Loss_{Test}$), trajectories (dashed dark: exact flow, green: numerical flow with learned vector fields and local error (yellow) for the Van der Pol oscillator with Forward Euler method with Micro-Macro correction in the case $\varepsilon = 0.1$.

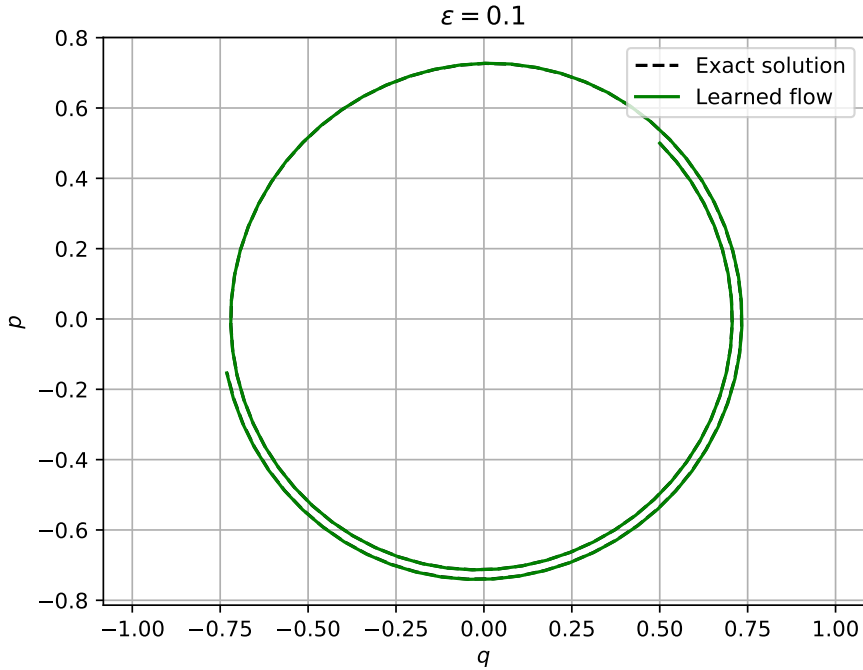


Figure 19: Comparison between trajectories (dashed dark: exact flow, green: numerical flow with learned vector field) for the Van der Pol oscillator with Forward Euler method with Micro-Macro correction in the case $\varepsilon = 0.1$ after the inverse variable change (49).

3.3 Error curves w.r.t. step size

We also investigate the global error between the exact flow and the numerical flow obtained from the learned vector fields. The errors are plotted as a function of the step size, with the curves showing perfect agreement with the estimates from the previous theorems (for the Forward Euler and Midpoint methods). Figures 20, 21, and 22 demonstrate that numerical integration using the micro-macro correction is more accurate than the *slow-fast* decomposition-based method, confirming the results obtained in subsection 3.2.

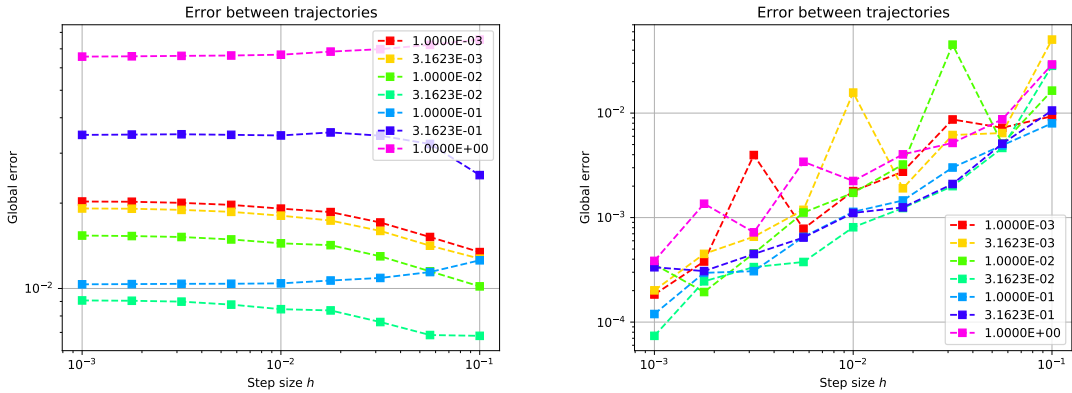


Figure 20: Integration errors (each color corresponds to a high oscillation parameter ε) of Inverted Pendulum with Forward Euler. Left: *Slow-fast* decomposition-based method. Right: With Micro-Macro correction.

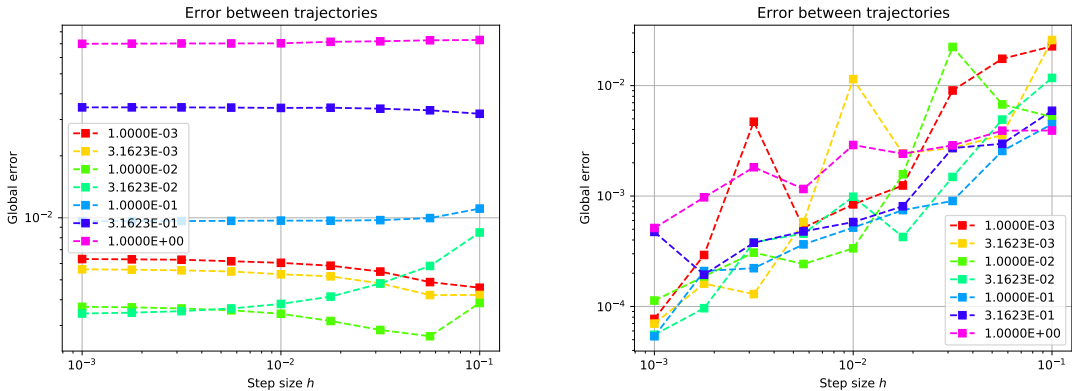


Figure 21: Integration errors (each color corresponds to a high oscillation parameter ε) of Inverted Pendulum with midpoint. Left: *Slow-fast* decomposition-based method. Right: With Micro-Macro correction.

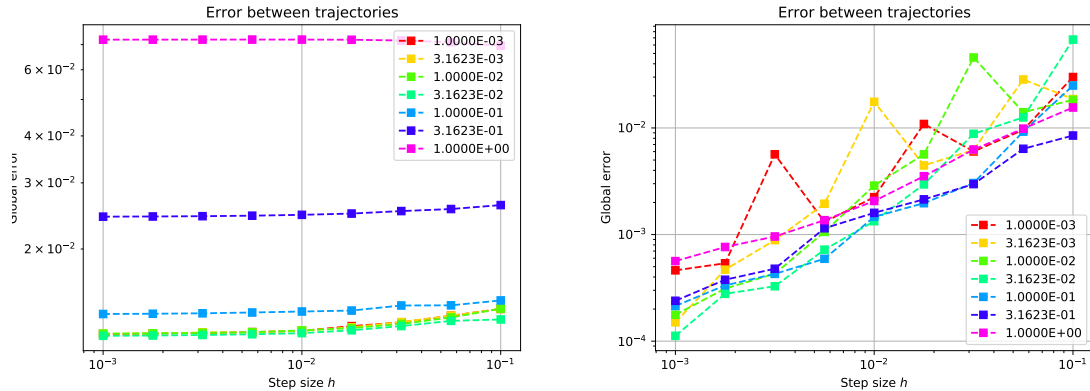


Figure 22: Integration errors (each color corresponds to a high oscillation parameter ε) of Van der Pol oscillator with Forward Euler. Left: *Slow-fast* decomposition-based method. Right: With Micro-Macro correction.

3.4 Uniform accuracy test

Since the micro-macro method is presented as a *uniformly accurate* (UA) method [14, 15], we can check whether the micro-macro correction with machine learning retains uniform accuracy by plotting the global errors against the parameter ε for various step sizes h .

Figures 23, 24, and 25 show that uniform accuracy is nearly verified with the micro-macro correction. However, this property is not observed with the *slow-fast* decomposition-based method, particularly for larger values of ε . This behavior can be attributed to the exponential remainder in the formula (5).

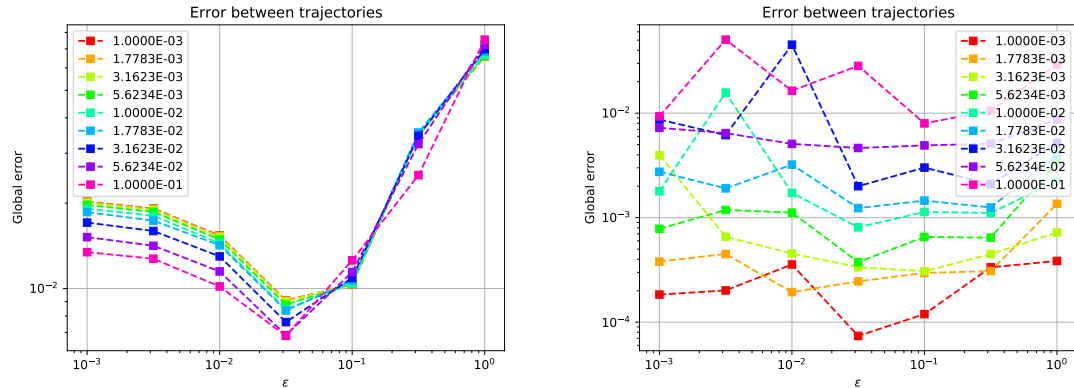


Figure 23: Uniform accuracy test (each color corresponds to a step size h) of Inverted Pendulum system with Forward Euler. Left: *Slow-fast* decomposition-based method. Right: With Micro-Macro correction.

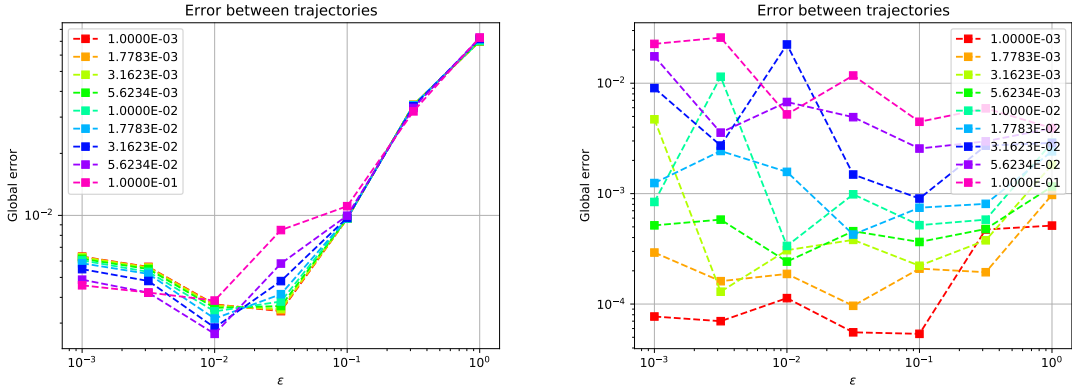


Figure 24: Uniform accuracy test (each color corresponds to a step size h) of Inverted Pendulum system with midpoint. Left: *Slow-fast* decomposition-based method. Right: With Micro-Macro correction.

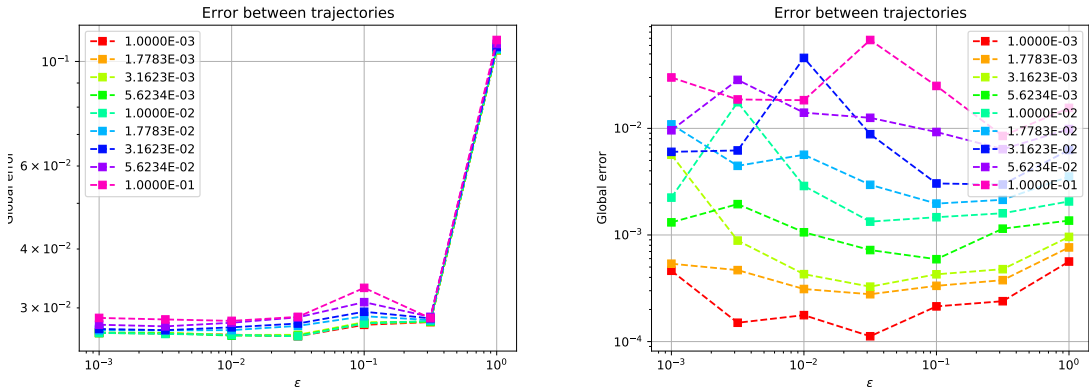


Figure 25: Uniform accuracy test (each color corresponds to a step size h) of Van der Pol oscillator with Forward Euler. Left: *Slow-fast* decomposition-based method. Right: With Micro-Macro correction.

3.5 Evaluation of alternative method

In this subsection, we compare the classical method using *slow-fast* decomposition with an alternative method in the autonomous case, using the Van der Pol oscillator as an example. Despite the absence of an auto-encoder, the classical method appears to yield more accurate solutions (as shown in Figures 26, 27, 28, and 29) than the alternative method (Figures 30 and 31). Furthermore, Figure 32 confirms the difference in accuracy.

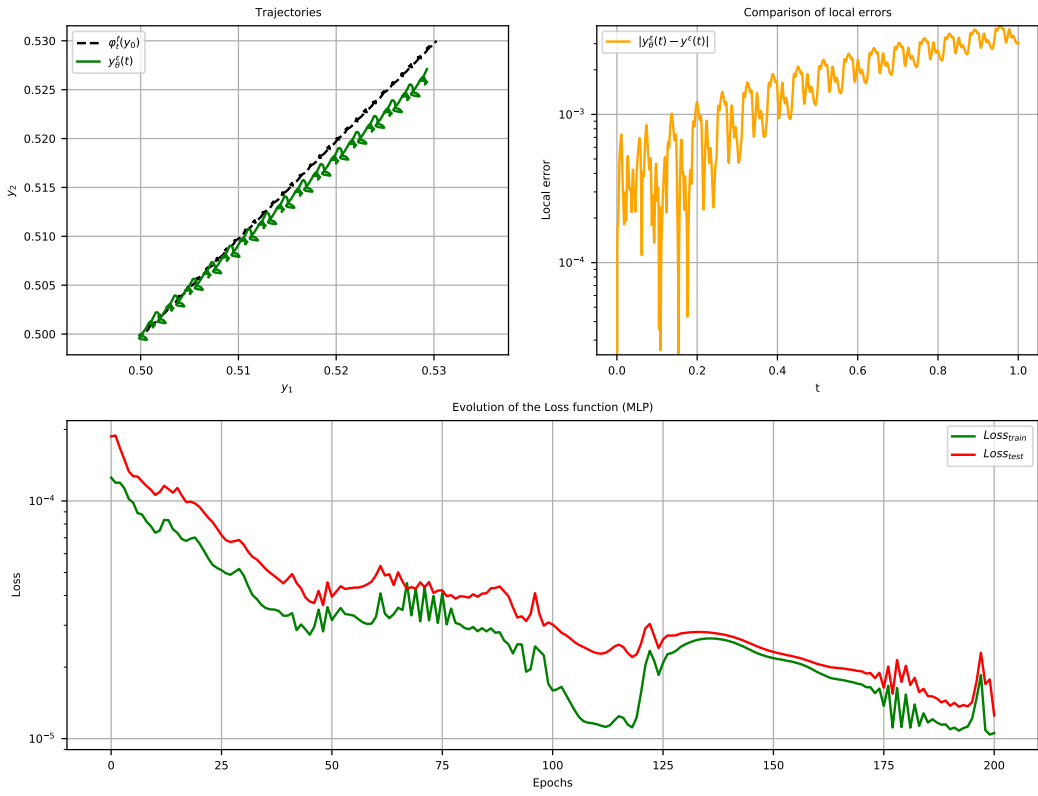


Figure 26: Comparison between *Loss* decays (green: $Loss_{Train}$, red: $Loss_{Test}$), trajectories (dashed dark: exact flow, green: numerical flow with learned vector fields and local error (yellow) for the Van der Pol oscillator with Forward Euler method in the case $\varepsilon = 0.01$.

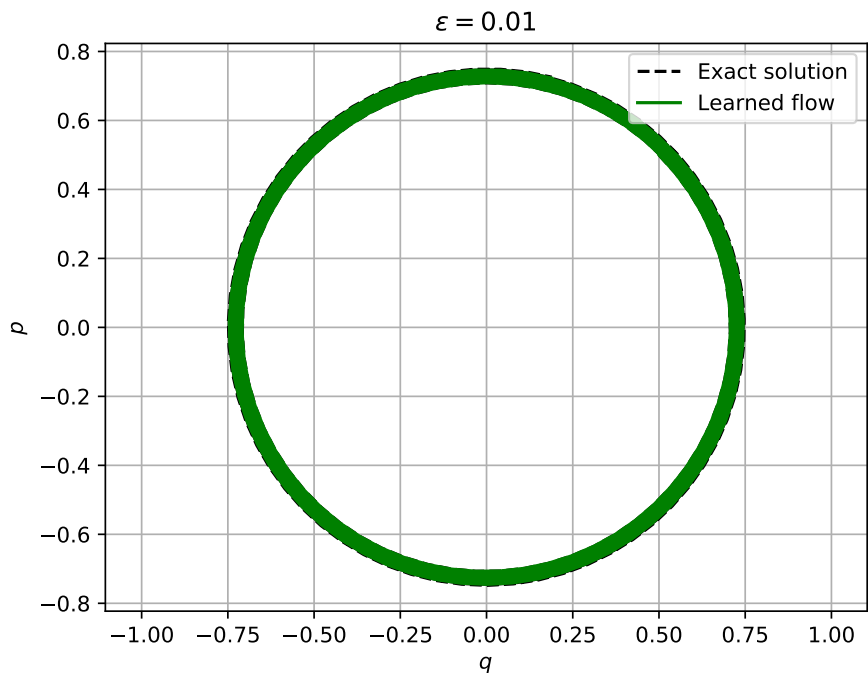


Figure 27: Comparison between trajectories (dashed dark: exact flow, green: numerical flow with learned vector field) for the Van der Pol oscillator with Forward Euler method in the case $\varepsilon = 0.01$ after the inverse variable change (49).

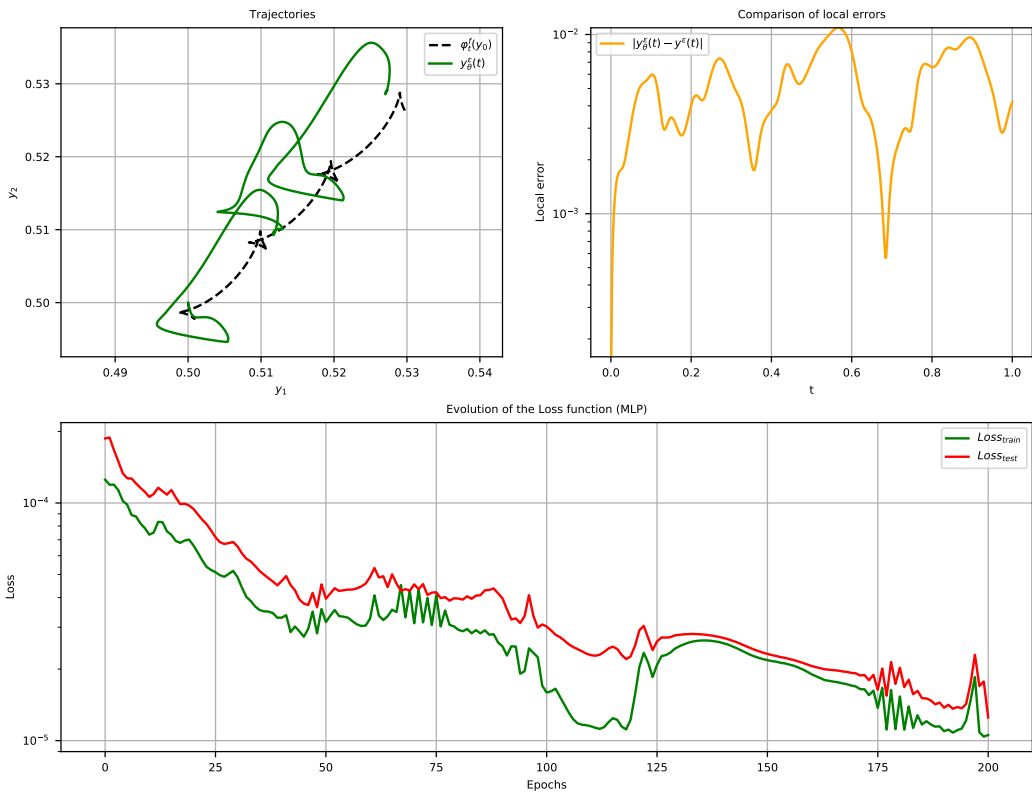


Figure 28: Comparison between *Loss* decays (green: $Loss_{Train}$, red: $Loss_{Test}$), trajectories (dashed dark: exact flow, green: numerical flow with learned vector fields and local error (yellow) for the Van der Pol oscillator with Forward Euler method in the case $\varepsilon = 0.1$.

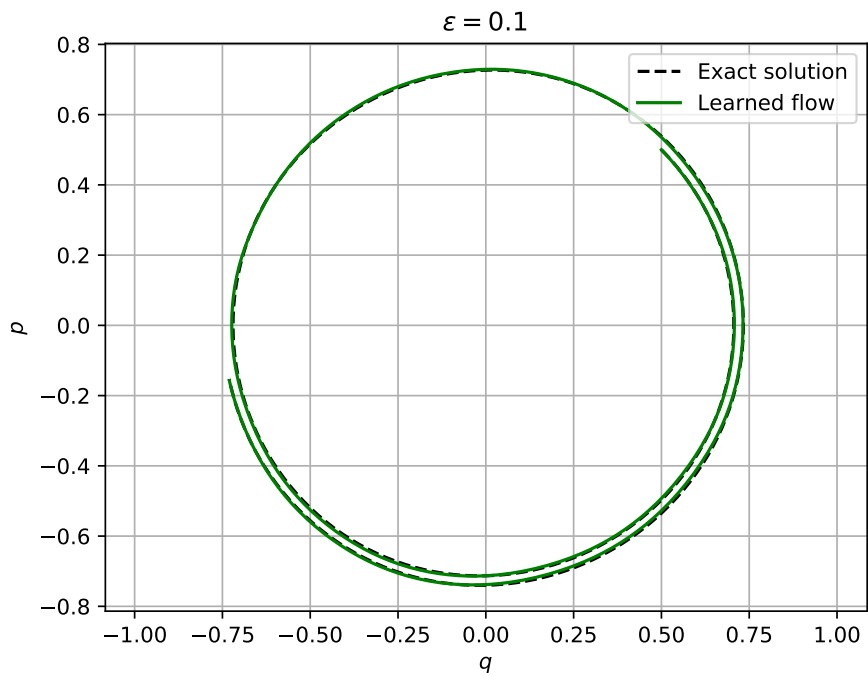


Figure 29: Comparison between trajectories (dashed dark: exact flow, green: numerical flow with learned vector field) for the Van der Pol oscillator with Forward Euler method in the case $\varepsilon = 0.1$ after the inverse variable change (49).

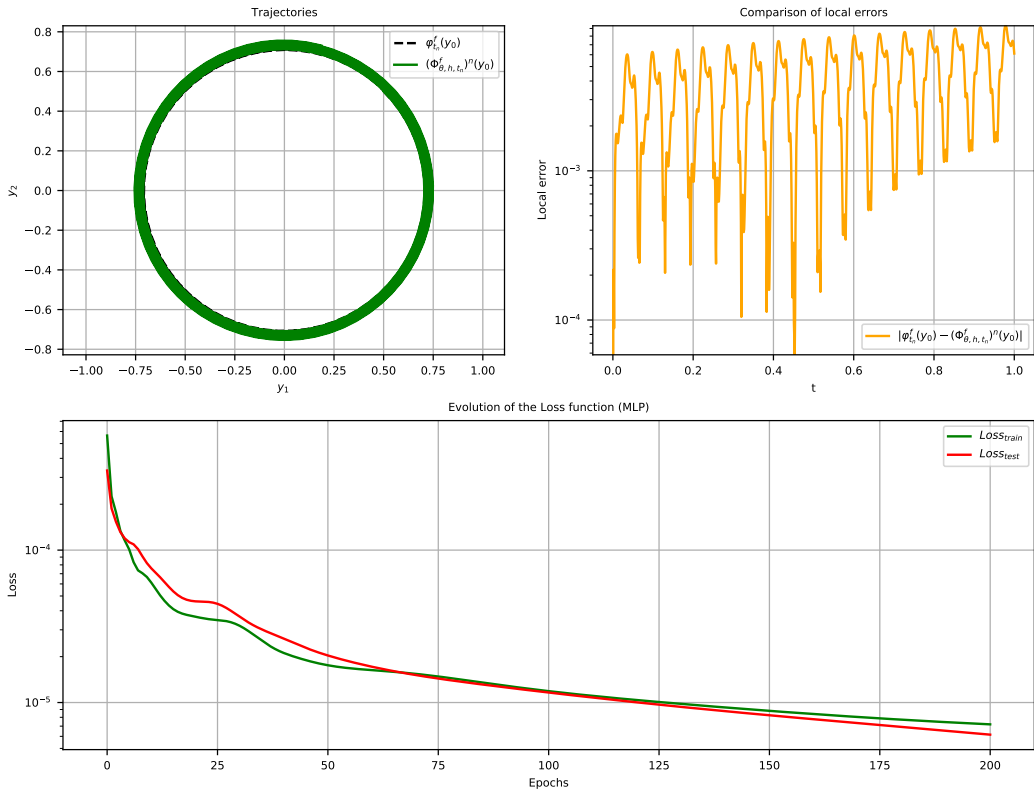


Figure 30: Comparison between *Loss* decays (green: $Loss_{Train}$, red: $Loss_{Test}$), trajectories (dashed dark: exact flow, green: numerical flow with learned vector fields and local error (yellow) for the Van der Pol oscillator with alternative method in the case $\varepsilon = 0.01$.

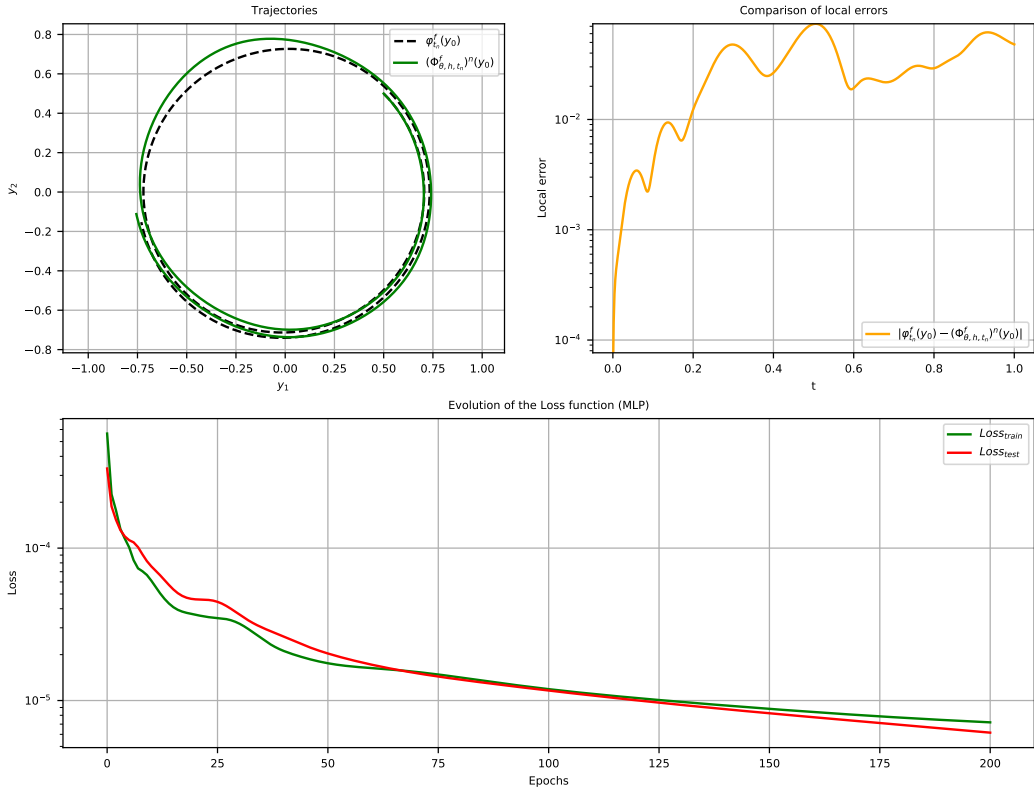


Figure 31: Comparison between *Loss* decays (green: $Loss_{Train}$, red: $Loss_{Test}$), trajectories (dashed dark: exact flow, green: numerical flow with learned vector fields and local error (yellow) for the Van der Pol oscillator with alternative method in the case $\varepsilon = 0.1$.

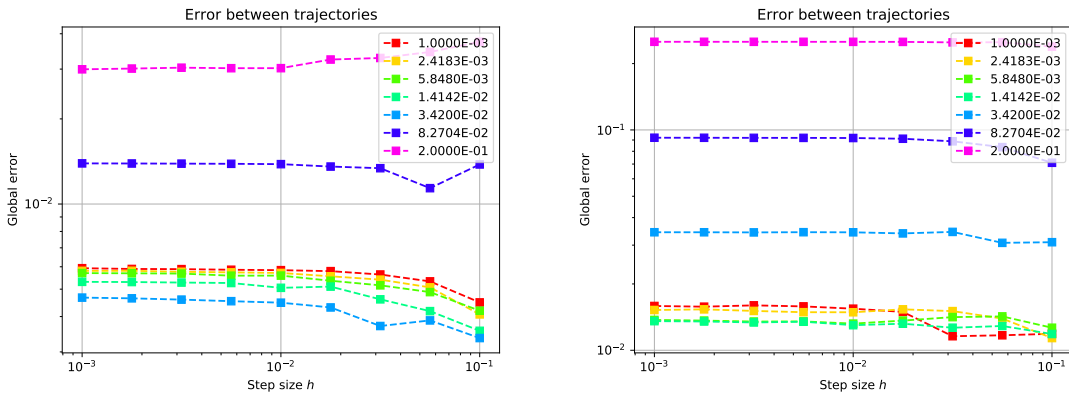


Figure 32: Integration errors (each color corresponds to a high oscillation parameter ε) of Van der Pol oscillator. Left: *Slow-fast* decomposition-based method. Right: Alternative method for autonomous case.

4 Conclusions

The numerical experiments presented in this paper demonstrate the feasibility of learning both the highly oscillatory generator and the averaged field using neural networks. Additionally, numerical integration without pre-computation provides accurate approximations of the exact solutions to highly oscillatory differential equations. While the method based on *slow-fast* decomposition is simpler and computationally less demanding than the micro-macro correction, it still achieves nearly uniform accuracy and consistency—though perfect uniform accuracy and consistency are limited by learning errors. Given the challenges of applying machine learning to high-dimensional problems, our methods are particularly well-suited for low-dimensional systems.

Acknowledgements

The author would like to thank Philippe Chartier, Mohamed Lemou and Florian Méhats for their guidance, valuable advice and careful reading of this work.

Bibliography

- [1] George A Anastassiou. *Quantitative approximations*. Chapman and Hall/CRC, 2000.
- [2] George A Anastassiou. General sigmoid based banach space valued neural network approximation. *J. Computational Analysis and Applications*, 31(4):520–534, 2023.
- [3] Francis Bach. *Learning Theory from First Principles*. Preparation, 2021.
- [4] Wolf-Jürgen Beyn, Luca Dieci, Nicola Guglielmi, Ernst Hairer, Jesús María Sanz-Serna, and Marino Zennaro. Current challenges in stability issues for numerical differential equations. *Cetraro: Springer*, 2011.
- [5] Maxime Bouchereau, Philippe Chartier, Mohammed Lemou, and Florian Méhats. Machine learning methods for autonomous ordinary differential equations. *Communications in Mathematical Sciences*, 2025.
- [6] Steven L Brunton, Joshua L Proctor, and J Nathan Kutz. Discovering governing equations from data by sparse identification of nonlinear dynamical systems. *Proceedings of the national academy of sciences*, 113(15):3932–3937, 2016.
- [7] John Charles Butcher. *Numerical methods for ordinary differential equations*. John Wiley & Sons, 2016.
- [8] Jean-Eric Campagne. Les réseaux de neurones multi-couches: le comment et le pourquoi, 2019. Notes et commentaires au sujet des conférences de S. Mallat du Collège de France.
- [9] Fernando Casas and Vicente Martínez. *Advances in Differential Equations and Applications*. Springer, 2014.

- [10] Philippe Chartier, Ander Murua, and Jesus Maria Sanz-Serna. Higher-order averaging, formal series and numerical integration i: B-series. *Foundations of Computational Mathematics*, 10(6):695–727, 2010.
- [11] Philippe Chartier, Ander Murua, and Jesus Maria Sanz-Serna. A formal series approach to averaging: exponentially small error estimates. *Discrete and Continuous Dynamical Systems-Series A*, 32(9), 2012.
- [12] Philippe Chartier, Ander Murua, and Jesus Maria Sanz-Serna. Higher-order averaging, formal series and numerical integration iii: error bounds. *Foundations of Computational Mathematics*, 15:591–612, 2015.
- [13] Philippe Chartier, Nicolas Crouseilles, Mohammed Lemou, and Florian Méhats. Averaging of highly-oscillatory transport equations. *Kinetic and Related Models*, 13(6):1107–1133, 2020.
- [14] Philippe Chartier, Mohammed Lemou, Florian Méhats, and Gilles Vilmart. A new class of uniformly accurate numerical schemes for highly oscillatory evolution equations. *Foundations of Computational Mathematics*, 20:1–33, 2020.
- [15] Philippe Chartier, Mohammed Lemou, Florian Méhats, and Xiaofei Zhao. Derivative-free high-order uniformly accurate schemes for highly oscillatory systems. *IMA Journal of Numerical Analysis*, 42(2):1623–1644, 2022.
- [16] Clémentine Courtès, Emmanuel Franck, Michael Kraus, Laurent Navoret, and Léopold Trémant. Neural non-canonical hamiltonian dynamics for long-time simulations. *arXiv preprint arXiv:2510.01788*, 2025.
- [17] Marco David and Florian Méhats. Symplectic learning for hamiltonian neural networks. *Journal of Computational Physics*, 494:112495, 2023.
- [18] Tim De Ryck, Samuel Lanthaler, and Siddhartha Mishra. On the approximation of functions by tanh neural networks. *Neural Networks*, 143:732–750, 2021.
- [19] Qiang Du, Yiqi Gu, Haizhao Yang, and Chao Zhou. The discovery of dynamics via linear multistep methods and deep learning: error estimation. *SIAM Journal on Numerical Analysis*, 60(4):2014–2045, 2022.
- [20] Samuel Greydanus, Misko Dzamba, and Jason Yosinski. Hamiltonian neural networks. *Advances in neural information processing systems*, 32, 2019.
- [21] Rémi Gribonval, Gitta Kutyniok, Morten Nielsen, and Felix Voigtlaender. Approximation spaces of deep neural networks. *Constructive Approximation*, 55(1):259–367, 2022.
- [22] Ernst Hairer, Syvert P Nørsett, and Gerhard Wanner. *Solving Ordinary Differential Equations I*. Springer Berlin Heidelberg, second edition, 1993. ISBN 978-3-540-56670-0.
- [23] Ernst Hairer, Christian Lubich, and Gerhard Wanner. *Geometric Numerical Integration*. 03 2010. ISBN 9783642051579.

[24] Pengzhan Jin, Zhen Zhang, Ioannis G Kevrekidis, and George Em Karniadakis. Learning poisson systems and trajectories of autonomous systems via poisson neural networks. *IEEE Transactions on Neural Networks and Learning Systems*, 2022.

[25] Shi Jin, Zheng Ma, and Keke Wu. Asymptotic-preserving neural networks for multiscale time-dependent linear transport equations. *Journal of Scientific Computing*, 94(3):57, 2023.

[26] Benedict Leimkuhler and Sebastian Reich. *Simulating hamiltonian dynamics*. Number 14. Cambridge university press, 2004.

[27] Wing Tat Leung, Guang Lin, and Zecheng Zhang. Nh-pinn: Neural homogenization-based physics-informed neural network for multiscale problems. *Journal of Computational Physics*, 470:111539, 2022.

[28] Yulong Lu, Li Wang, and Wuzhe Xu. Solving multiscale steady radiative transfer equation using neural networks with uniform stability. *Research in the Mathematical Sciences*, 9(3):45, 2022.

[29] Duong Nguyen, Said Ouala, Lucas Drumetz, and Ronan Fablet. Em-like learning chaotic dynamics from noisy and partial observations. *arXiv preprint arXiv:1903.10335*, 2019.

[30] Christian Offen and Sina Ober-Blöbaum. Symplectic integration of learned hamiltonian systems. *Chaos: An Interdisciplinary Journal of Nonlinear Science*, 32(1):013122, 2022.

[31] Lawrence M Perko. Higher order averaging and related methods for perturbed periodic and quasi-periodic systems. *SIAM Journal on Applied Mathematics*, 17(4):698–724, 1969.

[32] Peter J Prince and John R Dormand. High order embedded runge-kutta formulae. *Journal of computational and applied mathematics*, 7(1):67–75, 1981.

[33] Maziar Raissi, Paris Perdikaris, and George Em Karniadakis. Machine learning of linear differential equations using gaussian processes. *Journal of Computational Physics*, 348:683–693, 2017.

[34] Yuting Weng and Dezhi Zhou. Multiscale physics-informed neural networks for stiff chemical kinetics. *The Journal of Physical Chemistry A*, 126(45):8534–8543, 2022.

[35] Keke Wu, Xiong-Bin Yan, Shi Jin, and Zheng Ma. Capturing the diffusive behavior of the multiscale linear transport equations by asymptotic-preserving convolutional deeponets. *Computer Methods in Applied Mechanics and Engineering*, 418:116531, 2024.

[36] Aiqing Zhu, Pengzhan Jin, Beibei Zhu, and Yifa Tang. Inverse modified differential equations for discovery of dynamics. *arXiv preprint arXiv:2009.01058*, 2020.

[37] Aiqing Zhu, Beibei Zhu, Jiawei Zhang, Yifa Tang, and Jian Liu. Vpnets: Volume-preserving neural networks for learning source-free dynamics. *arXiv preprint arXiv:2204.13843*, 2022.

A Proof of theorem 1

Let $t \mapsto \psi_t^\varepsilon$ represent the exact solution of the autonomous differential equation associated with the vector field $F^{\varepsilon, [n_\varepsilon]}$. Additionally, let $\psi_{\theta, n}^\varepsilon$ denote the corresponding numerical flow:

$$\begin{cases} \psi_{\theta, 0}^\varepsilon &= y^\varepsilon(0) \\ \psi_{\theta, n+1}^\varepsilon &= \Phi_h^{F_\theta(\cdot, h, \varepsilon)}(\psi_{\theta, n}^\varepsilon) \end{cases} \quad (56)$$

First, we examine the estimates over this autonomous ODE. Then a general error estimate is provided.

(i). Consistency error (autonomous ODE): Consistency error is given by

$$\begin{aligned} \varepsilon_{\theta, n} &:= \psi_{t_{n+1}}^\varepsilon - \Phi_h^{F_\theta(\cdot, h, \varepsilon)}(\psi_{t_n}^\varepsilon) \\ &= \varphi_h^{F^{\varepsilon, [n_\varepsilon]}}(\psi_{t_n}^\varepsilon) - \Phi_h^{\widetilde{F^{\varepsilon, [n_\varepsilon], [q]}}}(\psi_{t_n}^\varepsilon) + \Phi_h^{\widetilde{F^{\varepsilon, [n_\varepsilon], [q]}}}(\psi_{t_n}^\varepsilon) - \Phi_h^{F_\theta(\cdot, h, \varepsilon)}(\psi_{t_n}^\varepsilon) \end{aligned} \quad (57)$$

According to the first hypothesis of theorem 1, we obtain

$$|\varepsilon_{\theta, n}| \leq \bar{C}h^{p+q} + C\delta_F h \quad (58)$$

(ii). Local truncation error (autonomous ODE): Local truncation error is given by

$$e_{\theta, n} := \psi_{\theta, n}^\varepsilon - \psi_{t_n}^\varepsilon. \quad (59)$$

Thus we have

$$e_{\theta, n+1} = \Phi_h^{F_\theta(\cdot, h, \varepsilon)}(\psi_{\theta, n}^\varepsilon) - \Phi_h^{F_\theta(\cdot, h, \varepsilon)}(\psi_{t_n}^\varepsilon) - \varepsilon_{\theta, n}. \quad (60)$$

Thus there exists a constant λ (the Lipschitz constant of F_θ with respect to its space variable) such that

$$|e_{\theta, n+1}| \leq (1 + \lambda h)|e_{\theta, n}| + \bar{C}h^{p+q} + C\delta_F h. \quad (61)$$

Using the discrete Grönwall lemma we obtain

$$\max_{0 \leq n \leq N} |e_{\theta, n}| \leq \frac{e^{\lambda T} - 1}{\lambda} \left[\bar{C}h^{p+q-1} + C\delta_F \right] \quad (62)$$

(iii). General error estimate: Let us consider and denote $\eta_{\theta, n}$ as the following error

$$\begin{aligned} \eta_{\theta, n} &:= y^\varepsilon(t_n) - y_{\theta, n}^\varepsilon \\ &= y^\varepsilon(t_n) - \phi_{\theta, +} \left(\frac{t_n}{\varepsilon}, \psi_{\theta, n}^\varepsilon, \varepsilon \right). \end{aligned} \quad (63)$$

By employing the following decomposition:

$$\begin{aligned}\eta_{\theta,n} &= y^\varepsilon(t_n) - \phi_{\frac{t_n}{\varepsilon}}^{\varepsilon, [n_\varepsilon]}(\psi_{t_n}^\varepsilon) + \phi_{\frac{t_n}{\varepsilon}}^{\varepsilon, [n_\varepsilon]}(\psi_{t_n}^\varepsilon) - \phi_{\theta,+}\left(\frac{t_n}{\varepsilon}, \psi_{t_n}^\varepsilon, \varepsilon\right) \\ &\quad + \phi_{\theta,+}\left(\frac{t_n}{\varepsilon}, \psi_{t_n}^\varepsilon, \varepsilon\right) - \phi_{\theta,+}\left(\frac{t_n}{\varepsilon}, \psi_{\theta,n}^\varepsilon, \varepsilon\right),\end{aligned}\quad (64)$$

we bound the first, second and third terms from above using (5), the learning error $\delta_{\phi,+}$ and the estimate for $e_{\theta,n}$. This will provide the desired estimate.

B Proof of theorem 2

1. Error estimate for $v_{\theta,n}$:

For the estimate of v , we apply a classical error estimation technique commonly used for autonomous differential equations, similar to the estimation of the autonomous part in the proof of 1.

(i). Consistency Error: Consistency error is given by

$$\begin{aligned}\varepsilon_{\theta,v,n} &:= v(t_{n+1}) - \Phi_h^{F_\theta(\cdot, h, \varepsilon)}(v(t_n)) \\ &= \varphi_h^{F^{[p]}}(v(t_n)) - \widehat{\Phi_h^{F^{[p], [q]}}}(v(t_n)) + \widehat{\Phi_h^{F^{[p], [q]}}}(v(t_n)) - \Phi_h^{F_\theta(\cdot, h, \varepsilon)}(v(t_n))\end{aligned}\quad (65)$$

according to the first hypothesis of Theorem 2 we obtain

$$|\varepsilon_{\theta,v,n}| \leq \bar{C}h^{p+q} + C\delta_F h. \quad (66)$$

(ii). Local Truncation Error: Local truncation error is given by

$$e_{\theta,v,n} := v(t_n) - v_{\theta,n}. \quad (67)$$

Therefore, we have

$$\begin{aligned}e_{\theta,v,n+1} &:= v(t_{n+1}) - v_{\theta,n+1} \\ &= \Phi_h^{F_\theta(\cdot, h, \varepsilon)}(v(t_n)) - \Phi_h^{F_\theta(\cdot, h, \varepsilon)}(v_{\theta,n}) + \varepsilon_{\theta,v,n}.\end{aligned}\quad (68)$$

Thus, there exists a constant λ (the Lipschitz constant of F_θ w.r.t. space variable) such that:

$$|e_{\theta,v,n+1}| \leq (1 + \lambda h)|e_{\theta,v,n}| + \bar{C}h^{p+q} + C\delta_F h. \quad (69)$$

By applying the discrete Grönwall lemma, we obtain

$$\max_{0 \leq n \leq N} |e_{\theta,v,n}| \leq \frac{e^{\lambda T} - 1}{\lambda} \left[\bar{C} h^{p+q-1} + C \delta_F \right] \quad (70)$$

2. Error estimate for $w_{\theta,n}$:

For the estimate of w , we treat v as a source term and perform an error estimation similar to the approach used for autonomous differential equations.

(i). Consistency Error: Consistency error is given by

$$\begin{aligned} \varepsilon_{\theta,w,n} &:= w(t_{n+1}) - \Phi_h^{g_\theta(\frac{t_n}{\varepsilon}, \cdot, v(t_n))} w(t_n) \\ &= \underbrace{w(t_{n+1}) - \Phi_{t_n,h}^{g(\frac{t_n}{\varepsilon}, \cdot, v(t_n))} w(t_n)}_{\text{Consistency error for classical scheme}} + \Phi_{t_n,h}^{g(\frac{t_n}{\varepsilon}, \cdot, v(t_n))} w(t_n) - \Phi_{t_n,h}^{g_\theta(\frac{t_n}{\varepsilon}, \cdot, v(t_n))} w(t_n). \end{aligned} \quad (71)$$

Since the first term can be bounded from above by Mh^{p+1} (where M is a constant independent of h and ε), and the second term can be bounded from above using the first hypothesis of theorem 2, we obtain

$$|e_{\theta,w,n}| \leq M'h^{p+1} + C\delta_g h \quad (72)$$

(ii). Local Truncation Error: Local truncation error is given by

$$e_{\theta,w,n} = w(t_n) - w_{\theta,n}. \quad (73)$$

Therefore, we have

$$\begin{aligned} e_{\theta,w,n+1} &= w(t_{n+1}) - w_{\theta,n+1} \\ &= \Phi_{t_n,h}^{g_\theta(\frac{t_n}{\varepsilon}, \cdot, v(t_n))} (w(t_n)) - \Phi_{t_n,h}^{g_\theta(\frac{t_n}{\varepsilon}, \cdot, v_{\theta,n})} (w_{\theta,n}) + \varepsilon_{\theta,w,n} \\ &= \Phi_{t_n,h}^{g_\theta(\frac{t_n}{\varepsilon}, \cdot, v(t_n))} (w(t_n)) - \Phi_{t_n,h}^{g_\theta(\frac{t_n}{\varepsilon}, \cdot, v_{\theta,n})} (w(t_n)) \\ &\quad + \Phi_{t_n,h}^{g_\theta(\frac{t_n}{\varepsilon}, \cdot, v_{\theta,n})} (w(t_n)) - \Phi_{t_n,h}^{g_\theta(\frac{t_n}{\varepsilon}, \cdot, v_{\theta,n})} (w_{\theta,n}) \\ &\quad + \varepsilon_{\theta,w,n} \end{aligned} \quad (74)$$

The first term can be bounded from above using the first hypothesis of theorem 2, while the second term can be estimated by introducing μ , the Lipschitz constant of g_θ , and applying the second hypothesis of theorem 2. Thus we obtain

$$\begin{aligned}
|e_{\theta,w,n+1}| &\leq Ch \left\| g_\theta \left(\frac{t_n}{\varepsilon}, \cdot, v(t_n) \right) - g_\theta \left(\frac{t_n}{\varepsilon}, \cdot, v_{\theta,n} \right) \right\|_{L^\infty(\Omega)} \\
&\quad + (1 + \mu h) |e_{\theta,w,n}| + Mh^{p+1} + Q\delta_g h \\
&\leq C\beta h |e_{\theta,v,n}| + (1 + \mu h) |e_{\theta,w,n}| + M'h^{p+1} + C\delta_g h,
\end{aligned} \tag{75}$$

where β is the Lipschitz constant of g_θ with respect to v . Since $|e_{\theta,w,n}|$ can be bounded from above by using the error estimate for v , we obtain

$$\begin{aligned}
|e_{\theta,w,n+1}| &\leq (1 + \mu h) |e_{\theta,w,n}| + M'h^{p+1} \\
&\quad + h \left[\frac{e^{\lambda T} - 1}{\lambda} \beta (\bar{C}h^{p+q-1} + C\delta_F) + C\delta_g \right].
\end{aligned} \tag{76}$$

Using the discrete Grönwall lemma, we obtain

$$\max_{0 \leq n \leq N} |e_{\theta,w,n}| \leq \frac{e^{\mu T} - 1}{\mu} \left[M'h^p + \frac{e^{\lambda T} - 1}{\lambda} \beta (\bar{C}h^{p+q-1} + C\delta_F) + C\delta_g \right] \tag{77}$$

3. Error estimate for $y_{\theta,n}^\varepsilon$: Finally, we perform an error estimate over y using the formula (17) to describe our numerical method. Since we have

$$y_{\theta,n}^\varepsilon = \phi_{\theta,+} \left(\frac{t_n}{\varepsilon}, v_{\theta,n}, \varepsilon \right) + w_{\theta,n}, \tag{78}$$

The local truncation errors can be expressed as follows:

$$\begin{aligned}
e_{\theta,n} &:= y^\varepsilon(t_n) - y_{\theta,n}^\varepsilon \\
&= \phi_{\frac{t_n}{\varepsilon}}^{[p]}(v(t_n)) + w(t_n) - \phi_{\theta,+} \left(\frac{t_n}{\varepsilon}, v_{\theta,n}, \varepsilon \right) - w_{\theta,n} \\
&= \phi_{\frac{t_n}{\varepsilon}}^{[p]}(v(t_n)) - \phi_{\frac{t_n}{\varepsilon}}^{[p]}(v_{\theta,n}) + \phi_{\frac{t_n}{\varepsilon}}^{[p]}(v_{\theta,n}) - \phi_{\theta,+} \left(\frac{t_n}{\varepsilon}, v_{\theta,n}, \varepsilon \right) + w(t_n) - w_{\theta,n}.
\end{aligned} \tag{79}$$

The first difference term can be bounded from above using α_ϕ , the Lipschitz constant of $\phi^{[p]}$, while the second difference term can be estimated using the learning error for $\phi_{\theta,+}$. Therefore we obtain

$$|e_{\theta,n}| \leq \alpha_\phi |e_{\theta,v,n}| + \delta_{\phi,+} \varepsilon + |e_{\theta,w,n}| \tag{80}$$

and the desired estimate follows.

C Proof of theorem 3

A standard proof used for autonomous ODEs (consistency and local truncation error) gives the following result. If we denote $t \mapsto \psi_t^\varepsilon$, the solution associated with g^ε and define $\psi_{\theta,n}^\varepsilon = (\varphi_\theta(\cdot, h, \varepsilon))^n (y^\varepsilon(0))$, then:

$$|\psi_{t_n}^\varepsilon - \psi_{\theta,n}^\varepsilon| \leq \frac{e^{\lambda T} - 1}{\lambda} \delta \varphi, \quad (81)$$

where λ is the Lipschitz constant of $R_{\theta,\varphi}$ with respect to y .

Then, using the following decomposition:

$$\begin{aligned} y_{\theta,n}^\varepsilon - y^\varepsilon(t_n) &= \phi_\theta \left(\frac{t_n}{\varepsilon}, \psi_{\theta,n}^\varepsilon, \varepsilon \right) - \Phi_{\frac{t_n}{\varepsilon}}^\varepsilon \left(\psi_{\theta,n}^\varepsilon \right) \\ &+ \Phi_{\frac{t_n}{\varepsilon}}^\varepsilon \left(\psi_{\theta,n}^\varepsilon \right) - \Phi_{\frac{t_n}{\varepsilon}}^\varepsilon \left(\varphi_{t_n}^{g^\varepsilon} (y^\varepsilon(0)) \right) \\ &+ \phi_{\frac{t_n}{\varepsilon}}^\varepsilon \left(\varphi_{t_n}^{g^\varepsilon} (y^\varepsilon(0)) \right) - y^\varepsilon(t_n), \end{aligned} \quad (82)$$

Since the first term is bounded from above by $\delta \phi$, the second term is bounded from above by $L |\psi_{t_n}^\varepsilon - \psi_{\theta,n}^\varepsilon|$, where L is the Lipschitz constant of $\Phi_{\frac{t_n}{\varepsilon}}^\varepsilon$ w.r.t. space variable, and the third term is estimated by the exponential remainder, we get the desired estimate.

D Implementation of implicit methods

In the formula (14), the numerical flow takes the input $\phi_{\theta,-} \left(\frac{t_0}{\varepsilon}, y_0, \varepsilon \right)$. For implicit methods, however, the numerical flow is a function of both the input and the output. $\phi_{\theta,-} \left(\frac{t_0+h}{\varepsilon}, y_1, \varepsilon \right)$ is considered as the output, and if we consider, for example, the midpoint rule, we have

$$\Phi_h^{F_\theta(\cdot, h, \varepsilon)} \left(\phi_{\theta,-} \left(\frac{t_0}{\varepsilon}, y_0, \varepsilon \right) \right) = \phi_{\theta,-} \left(\frac{t_0}{\varepsilon}, y_0, \varepsilon \right) + h F_\theta \left(\frac{\phi_{\theta,-} \left(\frac{t_0}{\varepsilon}, y_0, \varepsilon \right) + \phi_{\theta,-} \left(\frac{t_0+h}{\varepsilon}, y_1, \varepsilon \right)}{2}, h, \varepsilon \right) \quad (83)$$

E Computation of learning errors

E.1 Space and time discretizations

To compute the learning error with respect to ε , we discretise the space and time domains. In the formulas (55) we make the following approximations:

$$\max_{y \in \Omega} |F_\theta(y, 0, \varepsilon) - F^{[k]}(y)| \approx \max_{0 \leq i \leq I} |F_\theta(y_i, \varepsilon) - F^{[k]}(y_i)| \quad (84)$$

and

$$\max_{(\tau, y) \in [0, 2\pi] \times \Omega} |\phi_{\theta,+}(\tau, y, \varepsilon) - \phi_\tau^{[k]}(y)| \approx \max_{0 \leq i \leq I, 0 \leq j \leq J} |\phi_{\theta,+}(\tau_j, y_i, \varepsilon)|. \quad (85)$$

where $\{y_i\}_{0 \leq i \leq I}$ and $\{\tau_j\}_{0 \leq j \leq J}$ are discretisations of Ω and $[0, 2\pi]$ respectively. In our simulations we set $I = 960 = 31^2 - 1$ (with $\Omega = [-2, 2]^2$ represented by the points $\{(y_{1,l_1}, y_{2,l_2})\}_{0 \leq l_1, l_2 \leq 30}$) and $J = 30$.

E.2 Intergals and derivatives representation

We also set $\phi^{[0]} = Id$ and $F^{[0]} = \langle f \rangle$ for order 0. For order 1 we take, by the following formulas, (52) and (53):

$$\phi_\tau^{[1]}(y) = y + \varepsilon \int_0^\tau f(\sigma, y) d\sigma \quad (86)$$

and

$$F^{[1]}(y) = \left(\frac{\partial \langle \phi^{[1]} \rangle}{\partial y}(y) \right)^{-1} \left\langle f \left(\cdot, \phi^{[1]}(y) \right) \right\rangle. \quad (87)$$

To compute an integral of the form $\int_a^b g(\sigma) d\sigma$, we use a Gauss quadrature with 10 points.

Additionally, to approximate the space derivative of a function $g : \mathbb{R}^2 \mapsto \mathbb{R}^2$ (Jacobian matrix), we use the following finite difference approximation:

$$\frac{\partial g}{\partial y}(y) = \frac{1}{2\eta} [g(y + \eta \cdot e_1) - g(y - \eta \cdot e_1) \quad g(y + \eta \cdot e_2) - g(y - \eta \cdot e_2)] + \mathcal{O}(\eta^2), \quad (88)$$

where e_1, e_2 are the two vectors of the canonical base of \mathbb{R}^2 .

Furthermore, if $g, F = \mathbb{R}^d \longrightarrow \mathbb{R}^d$, we can approximate the directional derivative $\frac{\partial g}{\partial y}(y)F(y)$ using this finite difference approximation:

$$\frac{\partial g}{\partial y}(y)F(y) = \frac{1}{2\eta} [g(y + \eta F(y)) - g(y - \eta F(y))] + \mathcal{O}(\eta^2). \quad (89)$$

We take $\eta = 10^{-5}$ in our case.

F Influence of learning error

We assess the impact of learning error on integration error, as discussed in Theorems 1, 2, and 3. To illustrate this property, we compare Uniform Accuracy (UA) tests after two trainings sessions, using different numbers of hidden layers and neurons with Micro-macro correction method. Figure 33 demonstrates that efficient learning leads to a reduction in integration error.

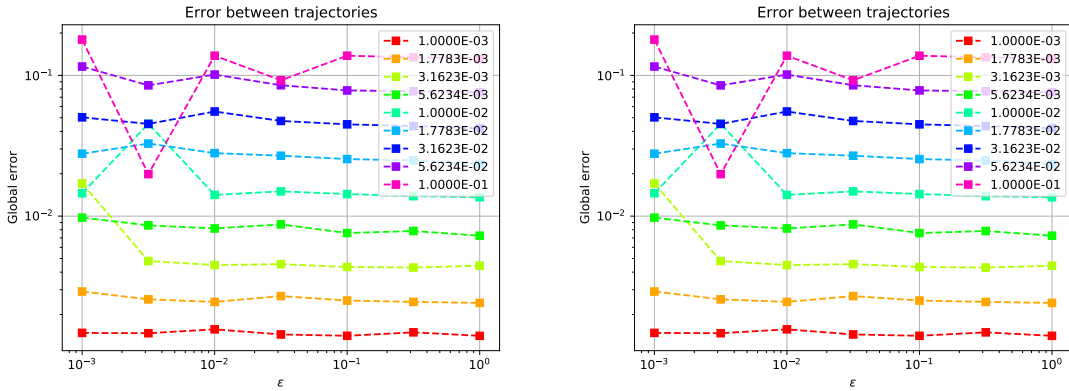


Figure 33: Influence of learning error over integration error (UA test) for Van der Pol oscillator. Left: $K = 800$ data, 25 neurons and 1 hidden layer per neural network. Right: $K = 500\,000$ data, 150 neurons and 2 hidden layers per neural network.

G Choice of the parameters

G.1 Inverted Pendulum - Forward Euler method

Parameters	
# Math Parameters:	
Dynamical system:	Inverted Pendulum
Numerical method:	Forward Euler
Interval where step sizes are selected:	$[h_-, h_+] = [10^{-3}, 10^{-1}]$
Interval where small parameters are selected:	$[\varepsilon_-, \varepsilon_+] = [10^{-3}, 1]$
Time for ODE simulation:	$T = 1$
step size for ODE simulation:	$h = 0.01$
High oscillation parameter for ODE simulation:	$\varepsilon \in \{5 \cdot 10^{-2}, 10^{-3}\}$
Initial datum:	$y^\varepsilon(0) = (0.5, -0.5)$
# Machine Learning Parameters:	
Domain where initial data are selected:	$\Omega = [-2, 2]^2$
Number of data:	$K = 1\,000\,000$
Proportion of data for training:	$80\% \cdot K_0 = 800\,000$
Batch size:	$B = 100$
Hidden layers per MLP:	2
Neurons on each hidden layer:	200
Learning rate:	$2 \cdot 10^{-3}$
Weight decay:	$1 \cdot 10^{-9}$
Epochs:	200

Computational time for data creation: 1 h 44 min 19 s

Computational time for training: 9 h 33 min 24s

G.2 Inverted Pendulum - midpoint method

Parameters	
# Math Parameters:	
Dynamical system:	Inverted Pendulum
Numerical method:	midpoint
Interval where step sizes are selected:	$[h_-, h_+] = [10^{-3}, 10^{-1}]$
Interval where small parameters are selected:	$[\varepsilon_-, \varepsilon_+] = [10^{-3}, 1]$
Time for ODE simulation:	$T = 1$
step size for ODE simulation:	$h = 0.01$
High oscillation parameter for ODE simulation:	$\varepsilon \in \{5 \cdot 10^{-2}, 10^{-3}\}$
Initial datum:	$y^\varepsilon(0) = (0.5, -0.5)$
# Machine Learning Parameters:	
Domain where initial data are selected:	$\Omega = [-2, 2]^2$
Number of data:	$K = 1\,000\,000$
Proportion of data for training:	$80\% \cdot K_0 = 800\,000$
Batch size:	$B = 100$
Hidden layers per MLP:	2
Neurons on each hidden layer:	200
Learning rate:	$2 \cdot 10^{-3}$
Weight decay:	$1 \cdot 10^{-9}$
Epochs:	200

Computational time for data creation: 1 h 44 min 19 s ⁴

Computational time for training: 9 h 11 min 8 s

G.3 Van der Pol oscillator - Forward Euler method

Parameters	
# Math Parameters:	
Dynamical system:	Van der Pol
Numerical method:	Forward Euler
Interval where step sizes are selected:	$[h_-, h_+] = [10^{-3}, 10^{-1}]$
Interval where small parameters are selected:	$[\varepsilon_-, \varepsilon_+] = [10^{-3}, 1]$
Time for ODE simulation:	$T = 1$
step size for ODE simulation:	$h = 0.01$ (for $\varepsilon = 0.1$) and $h = 0.001$ (for $\varepsilon = 0.01$)
High oscillation parameter for ODE simulation:	$\varepsilon \in \{10^{-1}, 10^{-2}\}$
Initial datum:	$y^\varepsilon(0) = (0.5, 0.5)$
# Machine Learning Parameters:	
Domain where initial data are selected:	$\Omega = [-2, 2]^2$
Number of data:	$K = 20\,000\,000$
Proportion of data for training:	$80\% \cdot K_0 = 16\,000\,000$
Batch size:	$B = 200$
Hidden layers per MLP:	2
Neurons on each hidden layer:	200
Learning rate:	$2 \cdot 10^{-3}$
Weight decay:	$1 \cdot 10^{-9}$
Epochs:	200

Computational time for data creation: 2 Days 8 h 2 min 30 s

Computational time for training: 3 Days 13 h 50 min 30 s

⁴data set used for Inverted Pendulum is the same for both Forward Euler and midpoint.

G.4 Van der Pol oscillator: Comparison between classical and alternative method

Parameters	
# Math Parameters:	
Dynamical system:	VDP
Interval where step sizes are selected:	$[h_-, h_+] = [10^{-3}, 10^{-1}]$
Interval where small parameters are selected:	$[\varepsilon_-, \varepsilon_+] = [10^{-3}, 0.2]$
Time for ODE simulation:	$T = 1$
step size for ODE simulation:	$h = 0.001$
Small parameter for ODE simulation:	$\varepsilon \in \{10^{-3}, 10^{-2}, 10^{-1}\}$
Initial datum:	$y^\varepsilon(0) = (0.5, 0.5)$
# Machine Learning Parameters:	
Domain where initial data are selected:	$\Omega = [-2, 2]^2$
Number of data:	$K = 100\,000$
Proportion of data for training:	80% - $K_0 = 80\,000$
Batch size:	$B = 100$
Hidden layers per MLP:	2
Neurons on each hidden layer:	200
Learning rate:	$2 \cdot 10^{-3}$
Weight decay:	$1 \cdot 10^{-9}$
Epochs:	200

- Classical method (with auto-encoder):

Computational time for data creation: 10 min 48 s

Computational time for training: 57 min 03 s

- Alternative method adapted for autonomous case:

Computational time for data creation: 10 min 52 s

Computational time for training: 48 min 47 s